

This discussion paper is/has been under review for the journal Biogeosciences (BG).
Please refer to the corresponding final paper in BG if available.

Late summer particulate organic carbon export and twilight zone remineralisation in the Atlantic sector of the Southern Ocean

F. Planchon^{1,2,3}, A.-J. Cavagna⁴, D. Cardinal^{3,5}, L. André³, and F. Dehaire⁴

¹Université Européenne de Bretagne, France

²Laboratoire des Sciences de l'Environnement Marin (LEMAR), Université de Brest, CNRS, IRD, UMR 6539, IUEM; Technopôle Brest Iroise, Place Nicolas Copernic, 29280 Plouzané, France

³Royal Museum for Central Africa, Geology Department, Tervuren, Belgium

⁴Vrije Universiteit Brussel, Analytical and Environmental Chemistry & Earth System Sciences, Brussels, Belgium

⁵Laboratoire d'Océanographie et du Climat : Expérimentations et Approches Numériques (LOCEAN), Université Pierre et Marie Curie, Paris, France

Received: 20 February 2012 – Accepted: 22 February 2012 – Published: 19 March 2012

Correspondence to: F. Planchon (frederic.planchon@univ-brest.fr)

Published by Copernicus Publications on behalf of the European Geosciences Union.

Title Page

Abstract

Introduction

Conclusions

References

Tables

Figures

◀

▶

◀

▶

Back

Close

Full Screen / Esc

Printer-friendly Version

Interactive Discussion



Abstract

During the Bonus-GoodHope (BGH) expedition (Jan–Mar 2008) we studied the water column distribution of total ^{234}Th and biogenic particulate Ba (Ba_{XS}) in the Atlantic sector of the Southern Ocean. The objective was to assess the export flux of particulate organic carbon (POC) from the surface to the mesopelagic twilight zone along a section between the Cape Basin and Weddell Gyre. Export production of POC was estimated from steady state and non steady state export fluxes of ^{234}Th which were converted into POC fluxes, using the $\text{POC}/^{234}\text{Th}$ ratio of large ($>53\ \mu\text{m}$) suspended particles, collected via in-situ pumps. Deficits in ^{234}Th activities were observed at all stations from the surface to the bottom of the mixed-layer. ^{234}Th export fluxes from the upper 100 m ranged from $496 \pm 57\ \text{dpm m}^{-2}\ \text{d}^{-1}$ to $1195 \pm 120\ \text{dpm m}^{-2}\ \text{d}^{-1}$ for the steady state model and from $149 \pm 18\ \text{dpm m}^{-2}\ \text{d}^{-1}$ to $1217 \pm 146\ \text{dpm m}^{-2}\ \text{d}^{-1}$ for the non steady state model calculated for a time window of 15 to 22 days preceding the timing of the present cruise. The $\text{POC}/^{234}\text{Th}_p$ ratio of large, potentially sinking particles ($>53\ \mu\text{m}$), was observed to increase with latitude, from $1.9 \pm 0.2\ \mu\text{mol dpm}^{-1}$ and $1.7 \pm 0.3\ \mu\text{mol dpm}^{-1}$ in the Subtropical Zone (STZ) and Subantarctic Zone (SAZ), respectively, to $3.0 \pm 0.2\ \mu\text{mol dpm}^{-1}$ in the Polar Front Zone (PFZ), $4.8 \pm 1.9\ \mu\text{mol dpm}^{-1}$ at the Southern Antarctic Circumpolar Current Front (SACCF) to $4.1 \pm 1.7\ \mu\text{mol dpm}^{-1}$ in the northern Weddell Gyre, in line with an increasing contribution of larger cell diatoms. Steady state and non steady state POC export from the upper 100 m ranged from $0.9 \pm 0.2\ \text{mmolC m}^{-2}\ \text{d}^{-1}$ to $5.1 \pm 2.1\ \text{mmolC m}^{-2}\ \text{d}^{-1}$ and from $0.3 \pm 0.0\ \text{mmolC m}^{-2}\ \text{d}^{-1}$ to $4.9 \pm 3.2\ \text{mmolC m}^{-2}\ \text{d}^{-1}$, respectively. From the SAZ to the SACCF, non steady state POC export production represented only 15 to 54 % of the steady state POC flux, suggesting that the intensity of export had decreased over time partly due to the fact that regenerated-production based communities of small-sized phytoplankton became predominant. In contrast, for the HNLC area south of the SACCF, we found an excellent agreement between the two modeling approaches indicating that surface POC export remained rather constant there.

Late summer particulate organic carbon export

F. Planchon et al.

Title Page

Abstract

Introduction

Conclusions

References

Tables

Figures



Back

Close

Full Screen / Esc

Printer-friendly Version

Interactive Discussion



Estimated POC export represented between 6 to 54 % of the potential export as represented by new production, indicating that export efficiency was particularly low throughout the studied area, except close to the SACCF.

Below the export layer, in the mesopelagic zone, ^{234}Th activities generally reached equilibrium with ^{238}U , but sometimes were in large excess relative to ^{238}U ($^{234}\text{Th}/^{238}\text{U}$ ratio > 1.1), reflecting intense remineralisation/disaggregation of ^{234}Th -bearing particles. The accumulation of excess ^{234}Th in the 100–600 m depth interval ranged from $458 \pm 55 \text{ dpm m}^{-2} \text{ d}^{-1}$ to $3068 \pm 368 \text{ dpm m}^{-2} \text{ d}^{-1}$. Using POC to ^{234}Th ratio of sinking particles, we converted this ^{234}Th flux into a POC remineralisation flux, which ranged between 0.9 to 9.2 $\text{mmolC m}^{-2} \text{ d}^{-1}$. Mesopelagic remineralisation was also evidenced by Ba_{xS} inventories which are related to bacterial degradation of sinking material and offer a means to quantify the flux of respired C. Highest biogenic particulate Ba (Ba_{xS}) contents were generally observed in the 200–400 m depth interval with values reaching up to $> 1000 \text{ pM}$ in the northern PFZ. Depth weighted average mesopelagic Ba_{xS} (meso- Ba_{xS}) was high in the PFZ and low in the northernmost (STZ-SAZ) and the southernmost (SACCF-AZ-WG) parts of the BGH section; conversion into respired C flux yielded a range of -0.23 to $6.4 \text{ mmolC m}^{-2} \text{ d}^{-1}$. Excluding two outliers, we found a significant positive correlation for mesopelagic waters between POC remineralisation estimated from meso- Ba_{xS} and from ^{234}Th excess ($R^2 = 0.73$). Our results indicate that POC export production in this area of the Southern Ocean was strongly attenuated in the mesopelagic waters due to remineralisation, a process which thus appears to strongly impact on longer term bathypelagic zone sequestration of POC.

1 Introduction

The exchange of carbon dioxide (CO_2) between the atmosphere and the ocean represents a critical feedback of the earth climatic system. The Southern Ocean (SO), which includes the circumpolar and polar gyres surrounding the Antarctic continent, is recognized for playing a central role in the global regulation of atmospheric CO_2 , at time

BGD

9, 3423–3477, 2012

Late summer particulate organic carbon export

F. Planchon et al.

Title Page

Abstract

Introduction

Conclusions

References

Tables

Figures

◀

▶

◀

▶

Back

Close

Full Screen / Esc

Printer-friendly Version

Interactive Discussion



scales varying from intra-annual, decadal, and up to glacial/interglacial fluctuations (de Boer et al., 2010; Gruber et al., 2009; Sigman et Boyle, 2000; Takahashi et al., 2009). High latitude CO₂ exchanges are driven by a combination of processes, which involve the large overturning circulation of Dissolved Inorganic Carbon (DIC) (solubility pump), and the production of sinking particles by marine organisms (biological pump). For the SO, carbon fixation through biological processes and transfer to the deep ocean as sinking Particulate Organic Carbon (POC) is considered a key sequestration mechanism. Indeed the SO is of particular interest since it is still under sampled compared to other oceanic basins and since SO has characteristics making it a key actor in the global carbon cycle due to physical (low temperature, high currents) and biogeochemical (a large reservoir of unused macronutrients) properties (e.g. Takahashi et al., 2009; Sarmiento et al., 2004). Therefore, during the last two decades the SO has been intensively studied in order to better quantify spatial and temporal variabilities (Boyd et Trull, 2007; Boyd, 2002; Buesseler et al., 2001, 2003; Rutgers van der Loeff et al., 1997; Trull et al., 2001, 2008). The subantarctic zone where the biological pump dominates the seasonal carbon budget has recently attracted renewed attention (Bowie et al., 2011; McNeil et Tilbrook, 2009).

Particle sinking rates in the SO are known to vary strongly according to season and geographical location. Such variability is reflected in the sedimentary record with high accumulation rates in the Opal Belt, a zone of 5–10° of latitude south of the Antarctic Polar Front, whereas low accumulation rates have been documented farther south, in the polar gyres, such as the Weddell Sea. However, since burial in abyssal sediments represents only a minor fraction (less than 1 % on average) of the sinking particle flux (Trull et al., 2008) it is therefore often considered to be decoupled from surface export production (Buesseler, 1998). This is especially the case for the SO, where carbon export production estimates based on ²³⁴Th activity measurements, new production measurements and seasonal nutrient budgets were shown to be significant although primary production is relatively low (Buesseler et al., 2001, 2009; Coppola et al., 2005; Friedrich et Rutgers van der Loeff, 2002; Nelson et al., 2002; Pondaven et al., 2000;

BGD

9, 3423–3477, 2012

**Late summer
particulate organic
carbon export**

F. Planchon et al.

Title Page

Abstract

Introduction

Conclusions

References

Tables

Figures

◀

▶

◀

▶

Back

Close

Full Screen / Esc

Printer-friendly Version

Interactive Discussion



Savoye et al., 2004b; Usbeck et al., 2002). A high surface export production, which can account for up to 30–50 % of the Net Primary Production (NPP), has been proposed to be partly related to seasonal blooms of diatoms (Rutgers van der Loeff et al., 1997, 2002). The usually observed strong decrease of C export flux with depth indicates intense attenuation of downward fluxes of biogenic particles (Martin et al., 1987). This was also supported by studies of the particulate barium distribution (Cardinal et al., 2005; Dehairs et al., 1997; Jacquet et al., 2008) and in a lesser extent observations about excess ^{234}Th activity (Savoye et al., 2004a; Usbeck et al., 2002), which help documenting the remineralization length scale for organic matter (OM) in SO meso-pelagic waters. Despite these substantial progresses, the SO remains an oceanic region largely unresolved in terms of observations and experiments, and therefore, large discrepancies between model estimates persist (Gruber et al., 2009; McNeil et al., 2007). Better constraining the processes that favor long-term sequestration of carbon in the Austral Ocean still represents a major scientific issue.

We report here new estimates of the POC export production from the Atlantic sector of the Southern Ocean, along a transect from the Cape Basin to the Northern Weddell gyre as part of the BONUS GoodHope (BGH) expedition (R/V *Marion Dufresne*) during the IPY 2008 (February-March 2008). The observed trends are discussed as a function of the successive frontal systems crossed by the BGH section between the Cape Basin and the northern Weddell Gyre.

The POC export fluxes were inferred from measurements of the short-lived radionuclide ^{234}Th ($t_{1/2} = 24.1$ d), which is now recognized as a robust proxy of the short-term dynamics of biogenic particles (Cochran and Masqué, 2003). Naturally occurring ^{234}Th is the decay product of ^{238}U , which is conservatively distributed in the open ocean, proportional to salinity (Chen et al., 1986; Pates and Muir, 2007). Unlike ^{238}U , ^{234}Th has a strong affinity for particulate matter and its activity distribution through the water column offers a means for quantifying export flux and aggregation/disaggregation of particles on regional and seasonal scales (Buesseler et al., 1992). Fluxes of ^{234}Th are combined with the measured ratio of $\text{POC}/^{234}\text{Th}$ of sinking particles in order to quantify

BGD

9, 3423–3477, 2012

**Late summer
particulate organic
carbon export**

F. Planchon et al.

Title Page

Abstract

Introduction

Conclusions

References

Tables

Figures

◀

▶

◀

▶

Back

Close

Full Screen / Esc

Printer-friendly Version

Interactive Discussion



upper ocean and mesopelagic export of POC (Cochran and Masqué, 2003; Maiti et al., 2010; Savoye et al., 2004a). We also report mesopelagic carbon remineralisation fluxes estimated from excess Ba (Ba_{xS} ; particulate Ba corrected for the lithogenic contribution). Ba_{xS} profiles in the open ocean are characterized by maximum concentrations in the upper mesopelagic (~150–500 m). This Ba_{xS} is mostly present under the form of micro-crystralline barite ($BaSO_4$) (Dehairs et al., 1980; Sternberg et al., 2008) and its formation is related to the decay of phytoplankton. Barite is precipitated in over-saturated micro-environments, mostly aggregates of organic material where bacterial activity is intense (Ganeshram et al., 2003). When micro-environments disintegrate and become remineralised in the mesopelagic zone, discrete barite crystals are released and the Ba_{xS} content can be related to carbon remineralisation activity (van Beek et al., 2009; Jacquet et al., 2008, 2011; Sternberg et al., 2008). The time-scale involved in this process represents a few days to a few weeks (Ganeshram et al., 2003; Cardinal et al., 2005; Jacquet et al., 2008) whereby short term variabilities are smoothed out.

2 Materials and methods

2.1 Study area

The cruise track of R/V *Marion Dufresne* during the BONUS GoodHope (BGH) expedition (8 February–24 March 2008) is shown in Fig. 1 together with the position of major hydrographic fronts encountered along the north to south transect between Cape Basin and northern Weddell Gyre. Starting from the subtropical domain, the cruise track crossed the southern subtropical front (S-STF), the sub-Antarctic front (SAF), the polar front (PF), the southern Antarctic circumpolar current front (SACCF), and finally the southern boundary of the ACC (Sbdy). Eleven stations were sampled for total ^{234}Th activity. Among these, five stations were also sampled for particulate ^{234}Th (S1 to S5) in order to obtain $\text{POC}/^{234}\text{Th}$ ratios of sinking particulate matter and derive POC export

BGD

9, 3423–3477, 2012

Late summer particulate organic carbon export

F. Planchon et al.

Title Page

Abstract

Introduction

Conclusions

References

Tables

Figures

◀

▶

◀

▶

Back

Close

Full Screen / Esc

Printer-friendly Version

Interactive Discussion



fluxes. Eight stations have been sampled for the Baxs proxy (S1 to S5 in addition to L3, L5 and L7).

2.2 Determination of total ^{234}Th activity

Total ^{234}Th activities were obtained from small volume (4 L) seawater samples collected from 12 L Niskin bottles. As detailed in Appendix 1, the samples for super stations (S1 to S5) were taken at 19–20 depths between the surface and 1000 m depth. For large stations L2 (41.18° S), L4 (46.02° S) and L6 (50.38° S), samples were collected at 5, 9 and 8 depths between surface and 300, 200 and 250 m depth, respectively. For large stations L3, L5 and L7, 15–17 samples were collected between the surface and 1000 m depth. For calibration purposes duplicate samples were taken at 1500 m depth at station S2 plus one other deep sample (2000 m) at L3.

Seawater samples were processed for total ^{234}Th activity measurement following the procedure developed by Pike et al. (2005). Samples were acidified to pH 2 using nitric acid and spiked with a known amount of ^{230}Th which serves as a yield monitor for ^{234}Th recovery. After 12 h equilibration the pH was raised to 8.5 using concentrated NH_4OH and Th was co-precipitated by adding 100 μL of MnCl_2 (2.0 g L^{-1}) and 100 μL of KMnO_4 (7.5 g L^{-1}). The samples were allowed to stand for 12 h before filtration on high-purity quartz microfiber filters (QMA, Sartorius; nominal pore size = 1 μm ; Ø 25 mm). Filtered samples were dried overnight, mounted on nylon filter holders and covered with Mylar film and Al foil. On board each sample was counted twice using a low level beta counter (RISØ, Denmark). Beta counting was allowed to proceed till counting uncertainty was below 2 % RSD. Residual beta activity was estimated for each sample after a delay of six ^{234}Th half-lives (~6 months) and was subtracted from the gross counts recorded on-board.

For Th recovery, filters were dismantled and MnO_2 precipitates dissolved in 10 ml 8M HNO_3 /10 % H_2O_2 solution and spiked with ^{229}Th as a second yield tracer. Dissolved samples were sonicated for 1 h, heated overnight (60 °C), filtered using Acrodisc

BGD

9, 3423–3477, 2012

Late summer particulate organic carbon export

F. Planchon et al.

Title Page

Abstract

Introduction

Conclusions

References

Tables

Figures

◀

▶

◀

▶

Back

Close

Full Screen / Esc

Printer-friendly Version

Interactive Discussion



0.2 μm syringe filters, and stored in clean 30 ml HDPE bottles, before analysis. Prior to analysis samples were diluted 10 to 20 times using 10 % nitric acid 10 % without any further purification. Determination of $^{230}\text{Th}/^{229}\text{Th}$ ratios was carried out by HR-ICP-MS (Element2, Thermo Electron) with low mass resolution settings ($M/\Delta M$: ~ 300) and hot plasma conditions (RF power: 1300 W). Samples were introduced in the plasma using a Peltier cooled (5°C) cyclonic spray chamber fitted with a $400\ \mu\text{L}\ \text{min}^{-1}$ glass micro nebulizer. Mass calibration and sensitivity tuning were carried out daily. Preliminary tests performed with standard solutions having a matrix similar to the samples in terms of Mn levels and spiked with ^{230}Th and ^{229}Th and digested using 8M $\text{HNO}_3/10\ \%\ \text{H}_2\text{O}_2$ showed that ICP-MS performances were unaffected by any matrix effect. Measurement uncertainty of $^{230}\text{Th}/^{229}\text{Th}$ ratios, in terms of Relative Standard Deviation (RSD), ranged from 0.1 to 1.6 % ($n = 3$ replicates) with dilution factors of 5 to 20. Estimated reproducibility of the method, evaluated with 9 standard solutions prepared separately and determined over different analytical sessions, was also particularly good and ranged from 0.5 to 1.3 %. The precision obtained with this simplified procedure meets the requirements defined by Pike et al. (2005), who emphasize the need to achieve $^{229}\text{Th}/^{230}\text{Th}$ ratio errors of $\leq 2\ \%$ in order to reach accurate ^{234}Th activities. Th recoveries were estimated for every sample processed ($n = 175$) and measurement precision as obtained from triplicate analyses were all below 2 % RSD. Average Th recovery was $87 \pm 2\ \%$ ($n = 175$). Uncertainties on total ^{234}Th activity are reported in Appendix 1 and represent on average $0.10\ \text{dpm}\ \text{L}^{-1}$. The parent ^{238}U activity was estimated with salinity measurements using the relationship of Pates and Muir (2007): $^{238}\text{U}\ (\text{dpm}\ \text{L}^{-1}) = (0.0713 \pm 0.0012) \cdot \text{Salinity}$. Overall accuracy of the method was evaluated from the deep water samples taken along the section between 1000 and 4400 m depth, and for which secular equilibrium between ^{234}Th and ^{238}U can reasonably be expected. Averaged $^{234}\text{Th}/^{238}\text{U}$ ratio for deep samples was 1.000 ± 0.031 ($n = 14$).

**Late summer
particulate organic
carbon export**

F. Planchon et al.

Title Page

Abstract

Introduction

Conclusions

References

Tables

Figures

◀

▶

◀

▶

Back

Close

Full Screen / Esc

Printer-friendly Version

Interactive Discussion



2.3 ²³⁴Th flux and models

²³⁴Th flux was estimated at 11 stations from total ²³⁴Th and ²³⁸U activities using a one-box model. The one-box model accounts for total ²³⁴Th activity balance (Savoie et al., 2006) and changes over time can be described using the following equation:

$$\frac{dA_{\text{Th}}}{dt} = \lambda A_{\text{U}} - \lambda A_{\text{Th}} - P + V \quad (1)$$

Where λ is the ²³⁴Th decay constant (0.0288 d⁻¹); A_{U} and A_{Th} represent total ²³⁸U and ²³⁴Th activities, respectively; P is the net loss of ²³⁴Th on sinking particles (i.e. vertical ²³⁴Th flux) expressed in dpm m⁻² d⁻¹, and V is the sum of the advective and diffusive fluxes.

If we neglect advective and diffuse fluxes ($V = 0$), the vertical flux of ²³⁴Th (P) can be estimated using the steady state (SS) approach ($\frac{dA_{\text{Th}}}{dt} = 0$)

In this study sites were not revisited over time (but see later) and therefore a first calculation was made using the SS assumption. In this case Eq. (1) can be simplified into:

$$P = \lambda(A_{\text{U}} - A_{\text{Th}}) \quad (2)$$

High resolution profiles of ²³⁴Th activity in the upper 1000 m allow the export flux to be estimated from the upper ocean (surface export) as well as from the mesopelagic zone at 600 m depth (mesopelagic export). Integration of ²³⁴Th activity along the water column was performed using a mid-point integration method.

²³⁴Th surface export flux was also estimated using the non steady state (NSS) model ($\frac{dA_{\text{Th}}}{dt} \neq 0$). This was possible because another cruise (ANTXXIV/3, R/V *Polastern*) preceded the BGH cruise by 14 to 22 days and followed exactly the same section (Zero Meridian). Sites with ²³⁴Th activities measured during the ANTXXIV/3 cruise matched with 6 out of the 11 sites sampled during BGH (Rutgers van der Loeff et al., 2011). ANTXXIV/3 results for these sites were considered initial ²³⁴Th activities for the

Title Page

Abstract

Introduction

Conclusions

References

Tables

Figures

◀

▶

◀

▶

Back

Close

Full Screen / Esc

Printer-friendly Version

Interactive Discussion



NSS approach. NSS export flux at 100 m was estimated using the following equation (Savoie et al., 2006):

$$P = \lambda \left[\frac{A_U(1 - e^{-\lambda\Delta t}) + A_{Th\ 1}e^{-\lambda\Delta t} - A_{Th\ 2}}{(1 - e^{\lambda\Delta t})} \right] \quad (3)$$

where Δt is the time interval between two successive occupations of a given site; $A_{Th\ 1}$ and $A_{Th\ 2}$ are the ^{234}Th activities for the first and second visit, respectively. This flux approach assumes that: (i) the same water mass is sampled during both visits; (ii) ^{238}U activity is constant, and (iii) diffusive and advective fluxes are negligible ($V=0$).

2.4 Measurements of particulate ^{234}Th and POC

For particulate ^{234}Th and POC, suspended particulate matter was collected at five stations (S1, S2, S3, S4 and S5) via in situ large-volume filtration (150–2000 L) systems (Challenger Oceanics and McLane WTS6-1-142LV pumps) equipped with 142 mm diameter filter holders. Two particle size classes ($>53\ \mu\text{m}$ and $53 \gg 1\ \mu\text{m}$) were collected via sequential filtration through a $53\ \mu\text{m}$ mesh nylon screen (filter SEFAR-PETEX®; polyester) and a $1\ \mu\text{m}$ pore size quartz fiber filter (QMA, Pall Life). Because suspended particles were also intended for other analyses by other participants, $^{14}\text{C}_{\text{POC}}$ and $^{210}\text{Pb}/^{210}\text{Po}$, biomarkers, the filters were pre-conditioned prior to sampling. The PETEX screens were soaked in HCl 5 %, rinsed with Milli-Q grade water, dried at ambient temperature in a laminar flow hood and stored in clean plastic bags. QMA filters were precombusted at 450°C during 4h and filters were stored in clean plastic bags before use.

After collection, filters were subsampled for the different end-users using sterile scalpels, a custom-build INOX steel support for $53\ \mu\text{m}$ PETEX screens and a plexiglass punch of 25 mm diameter for QMA filters. For large size particles ($>53\ \mu\text{m}$), particles on the PETEX screen parts dedicated to ^{234}Th were re-suspended in filtered seawater in a laminar flow hood, and collected on 25 mm diameter silver filters ($1.0\ \mu\text{m}$ porosity).

BGD

9, 3423–3477, 2012

Late summer particulate organic carbon export

F. Planchon et al.

Title Page

Abstract

Introduction

Conclusions

References

Tables

Figures

◀

▶

◀

▶

Back

Close

Full Screen / Esc

Printer-friendly Version

Interactive Discussion



Silver and QMA filters were dried overnight, and once mounted on nylon holders and covered with Mylar and Al foil were ready for beta counting. As for total ^{234}Th activity, particulate samples were counted twice on board until relative standard deviation was below 2%. Residual beta activity was measured in the home-based laboratory after six ^{234}Th half-lives (~6 months).

Following beta counting, particulate samples were processed for POC measurement by Elemental Analyzer - Isotope Ratio Mass Spectrometer (EA-IRMS). Size-fractionated samples were dismantled from filters holders and fumed under HCl vapor during 4 h inside a glass desiccator, to remove the carbonate phase. After overnight drying at 50 °C, samples were packed in silver cups and analyzed with a Carlo Erba NA 2100 elemental analyzer configured for C analysis and coupled on-line via a Con-Flo III interface to a Thermo-Finnigan Delta V isotope ratio mass spectrometer. Results obtained for C isotopic composition of POC are not included in this work. Acetanilide standard was used for C concentration calibration. C blanks were 0.98 μmol and 0.54 μmol for QMA and silver filters, respectively. Results obtained for bulk POC and two size-segregated POC fractions ($>53\ \mu\text{m}$ and $53\gg 1\ \mu\text{m}$) are reported in Table 1 along with particulate ^{234}Th activity measured on the same samples.

2.5 Ba_{XS} sampling and measurements

19–20 depths per station were sampled in the upper 1000 m using CTD rosette equipped with 12 L Niskin bottles. 5–10 L of seawater was filtered onto 0.4 μm polycarbonate membranes (\emptyset 90 mm for surface samples and 47 mm for the other depths) using large volume Perspex filtration units under slight overpressure supplied by filtered air (0.4 μm). Membranes were rinsed with a few mL of Milli-Q grade water to remove most of the sea salt, dried overnight in the oven at ~60 °C and then stored in plastic Petri dishes. Filtration blanks were prepared on-board by filtering 5 L of Milli-Q water and applying the same conditions as for samples.

Particles were digested with a tri-acid mixture (1.5 ml HCl 30%, 1.0 ml HNO_3 65% and 0.5 ml HF 40%, all Suprapur grade) in closed teflon beakers overnight at 90 °C,

Late summer particulate organic carbon export

F. Planchon et al.

Title Page

Abstract

Introduction

Conclusions

References

Tables

Figures

◀

▶

◀

▶

Back

Close

Full Screen / Esc

Printer-friendly Version

Interactive Discussion



were evaporated close to dryness and redissolved into ~13 ml of HNO₃ 2%. The solutions were analysed by ICP-MS X Series 2 (Thermo) equipped with a Collision Cell Technology (CCT). Ba, Na and Al contents were analysed simultaneously (with CCT for Al and without for Ba and Na). To check whether internal standards (⁹⁹Ru, ¹¹⁵In, ¹⁸⁷Re, ²⁰⁹Bi) adequately corrected possible matrix effects, we analysed several certified materials which also served to construct calibration curves. These standards solutions consisted of dilute acid-digested rocks (e.g. BHVO-1, GA, SGR-1), natural water (SLRS-4) and multi-element artificial solutions. Based on analyses of these standards, precision, accuracy and reproducibility are better than ± 5%. For more details on sample processing and analysis we refer to Cardinal et al. (2001). Detection limit in solution was calculated as three times the standard deviation of the on-board blanks and reaches 20 and 0.5 ppb for Al and Ba, respectively. BGH samples are largely exceeding this detection limit for Ba and on-board filtration blanks represented only 2 ± 0.8% of the average sample Ba content. For Al, 23 over a total of 160 samples are below detection limit (DL), but concentrations are most of the time very close to DL. Indeed, Al for on-board blanks represents 28 ± 14% of average sample Al content. However, this did not significantly affect the Ba_{xS} concentrations and the remineralisation fluxes, as discussed later.

Values of on-board prepared blanks were subtracted from sample values and excess Ba calculated by correcting total Ba for the lithogenic Ba contribution, using sample Al content and a Ba:Al crustal molar ratio of 0.00135 (Taylor et McLennan, 1985). Na was also analysed to correct any sea-salt contribution to Ba_{xS}. Remnant sea-salt was found to have but a negligible affect on Ba_{xS}.

2.6 Carbon fluxes calculations from Ba_{xS} depth profiles

Remineralisation carbon fluxes can be estimated using a relationship observed in ACC waters between meso-Ba_{xS} contents and the rate of oxygen consumption deduced

BGD

9, 3423–3477, 2012

Late summer particulate organic carbon export

F. Planchon et al.

Title Page

Abstract

Introduction

Conclusions

References

Tables

Figures

◀

▶

◀

▶

Back

Close

Full Screen / Esc

Printer-friendly Version

Interactive Discussion



from a 1-D advection diffusion model (Dehairs et al., 1997, 2008; Shopova et al., 1995):

$$J_{O_2} = (\text{mesoBa}_{xS} - \text{Ba}_{\text{residual}})/17450 \quad (4)$$

where J_{O_2} is the O_2 consumption ($\mu\text{mol l}^{-1} \text{d}^{-1}$), meso- Ba_{xS} is the observed depth-weighted average Ba_{xS} value in the upper mesopelagic waters (125 to 600 m depth interval) and $\text{Ba}_{\text{residual}}$ is the residual Ba_{xS} signal at zero oxygen consumption. For the BaSO_4 saturated water column of the ACC this residual Ba_{xS} was estimated to reach 180 pM (Monnin and Cividini, 2006; Monnin et al., 1999). Such value is expected also to prevail in deep waters (>600 m) where remineralisation is minimal compared to the upper mesopelagic. In the present study deep ocean Ba_{xS} values (800–1000 m) are generally close to 200 pM. This also holds for the deep SAZ and the STZ waters (stations S1, S2 and L3), known to be undersaturated for BaSO_4 (Monnin and Cividini, 2006; Monnin et al., 1999) and which therefore are expected to have smaller residual Ba_{xS} contents. Since that is not observed here, we choose to apply a single value of 180 pM for $\text{Ba}_{\text{residual}}$ at all stations.

Calculated J_{O_2} was then converted into carbon respired (C_{respired}) by:

$$C_{\text{respired}} = Z \times J_{O_2} \times RR \quad (5)$$

C_{respired} is the organic carbon remineralisation rate (in $\text{mmol C m}^{-2} \text{d}^{-1}$), Z is the thickness of the mesopelagic layer considered (i.e., $600-125 = 475 \text{ m}$), and RR is the Redfield C: O_2 molar ratio (125:175).

3 Results

3.1 $^{234}\text{Th}/^{238}\text{U}$ ratio profiles

The full data set, including activities of total ^{234}Th and ^{238}U , and corresponding $^{234}\text{Th}/^{238}\text{U}$ ratios can be found in Appendix 1. Figure 2 shows depth profiles of total $^{234}\text{Th}/^{238}\text{U}$ ratios in the upper 1000 m. The latitudinal section of $^{234}\text{Th}/^{238}\text{U}$ ratios

BGD

9, 3423–3477, 2012

Late summer particulate organic carbon export

F. Planchon et al.

Title Page

Abstract

Introduction

Conclusions

References

Tables

Figures

◀

▶

◀

▶

Back

Close

Full Screen / Esc

Printer-friendly Version

Interactive Discussion



in the upper 600 m is shown in Fig. 3a; From the Cape Basin to the northern Weddell Sea the surface waters appears clearly depleted in total ^{234}Th relative to its parent nuclide ^{238}U . Lowest $^{234}\text{Th}/^{238}\text{U}$ ratios (average 0.77 ± 0.04 , $n = 11$) are observed in the northern part of the section at stations S1 (36.5°S) and L2 (41.2°S) in the subtropical domain, and also at station S2 (42.3°S) and L3 (44.9°S) in the SAZ and PFZ, respectively. Southward in the PFZ, surface ^{234}Th deficits are much smaller with a mean $^{234}\text{Th}/^{238}\text{U}$ ratio of 0.84 ± 0.04 ($n = 23$) at stations L4 (46.2°S), S3 (47.5°S), and L5 (49.0°S). This trend goes along with substantial deepening of the surface ML which reaches 120 m at station L5. From the Polar Front (PF) at 50.4°S (station L6) to the northern part of the Weddell Gyre (WG) at 57.5°S (station S5), the surface depletion of total ^{234}Th diminishes further and the $^{234}\text{Th}/^{238}\text{U}$ ratio reaches a minimum value of 0.85 ± 0.04 ($n = 7$) south of the Southern Boundary (Sbdy) at S5.

Below the export layer ^{234}Th activity increases with depth and approaches equilibrium with ^{238}U at the bottom of the ML. At station S1 in the subtropical domain it is observed that after reaching equilibrium at the base of the ML (50 m depth) $^{234}\text{Th}/^{238}\text{U}$ ratio decreases again between at 80 and 100 m depth (Fig. 2). A depletion of ^{234}Th indicates loss of ^{234}Th via particle scavenging and suggests a surface origin for this 30 m thick, less saline (salinity = 34.9), subsurface water tongue. This may be related to the particular hydrography in this zone, where cyclonic eddies can contribute to the subduction of surface waters of westward origin (Chever et al., 2010; Gladyshev et al., 2008). Except for this particular feature at S1 it appears that deep total ^{234}Th activities in the subtropical zone (S1 and L2) are close to secular equilibrium with ^{238}U . However, south of the STF substantial deep ^{234}Th excess is observed in the PFZ at 44.9°S (station L3), at 46.0°S (station L4) and at 47.5°S (station S3), and also to some extent at 42.5°S in the SAZ (station S2). $^{234}\text{Th}/^{238}\text{U}$ activity ratios largely >1.1 clearly indicate substantial accumulation of ^{234}Th (i.e., excess ^{234}Th relative to ^{238}U) in the meso-pelagic zone, which can be attributed to particle remineralisation and/or disaggregation (Buesseler et al., 2008; Maiti et al., 2010; Savoye et al., 2004a). Between the PF at 50.4°S (station L6) and the Sbdy at 55.2°S (station L7) deep ^{234}Th activity

**Late summer
particulate organic
carbon export**F. Planchon et al.

Title Page

Abstract

Introduction

Conclusions

References

Tables

Figures

◀

▶

◀

▶

Back

Close

Full Screen / Esc

Printer-friendly Version

Interactive Discussion



returns to secular equilibrium. However, further south, in the northern part of the Weddell sea at 57.6° S (station S5) we again observe layers of excess ^{234}Th activity (just below the ML and at 250 m depth; see Fig. 2).

3.1.1 Export flux of ^{234}Th

(a) Surface export flux

The fluxes of ^{234}Th out of the surface layer (upper 100 m and at MLD) were calculated using steady state (SS) and non steady state (NSS) models (Table 2 and Fig. 4a). The steady state model calculations reveal that ^{234}Th export at 100 m varies from 565 dpm m⁻² d⁻¹ at 41.2° S (station L2, STZ) to 1195 dpm m⁻² d⁻¹ at 50.4° S (station L6, PF). When integrating the ^{234}Th flux over the depth of the ML rather than over a fixed depth (i.e. the upper 100 m), the SS export flux of ^{234}Th ranges from 388 to 1521 dpm m⁻² d⁻¹ and compares relatively well with the fluxes at 100 m. Differences arise for the stations located in the southern part of the ACC between 48° S and 55.2° S (PFZ to SACCF), where an important thickening of the ML (>100 m) is observed. At stations L5 (49.0° S) and S4 (51.9° S) the SS ^{234}Th export flux from the upper 100 m is about 30 % smaller than the flux from the ML. The SS export flux exhibits a latitudinal gradient which follows the structure of the upper ML (Fig. 4a). The smallest SS fluxes are observed in the STZ (stations S1 and L2), and also south of the ACC in the northern branch of the Weddell Sea Gyre (station S5) where the ML remains relatively shallow. ^{234}Th export is highest within the ACC, especially in its southern part between the PFZ to the AZ (stations S3 to L7), where the upper ML extends quite deep (80 to 120 m)

Although the steady state model is by far the most commonly used model in ^{234}Th export studies, the assumption of constant ^{234}Th activity with time is only valid for uniform scavenging conditions (constant export production) (Savoye et al., 2006). Such oversimplification prevents short-term processes to be explicitly considered and may not account properly for particle dynamics in specific conditions (e.g., blooms, eddies,

BGD

9, 3423–3477, 2012

Late summer particulate organic carbon export

F. Planchon et al.

Title Page

Abstract

Introduction

Conclusions

References

Tables

Figures

◀

▶

◀

▶

Back

Close

Full Screen / Esc

Printer-friendly Version

Interactive Discussion



etc). In our study, we also apply a non steady state (NSS) model to evaluate the ^{234}Th export flux, by making use of total ^{234}Th activity data that were obtained during another cruise (ANTXXIV/3, R/V *Polarstern*) along the Greenwich Meridian and which preceded the BHG cruise by 2 to 3 weeks (Rutgers van der Loeff et al., 2011). NSS ^{234}Th fluxes from the upper 100 m, (Fig. 4a) range from $149 \text{ dpm m}^{-2} \text{ d}^{-1}$ at 41.2° S (station S2, STZ) to $1217 \text{ dpm m}^{-2} \text{ d}^{-1}$ at 55.2° S (station L7, AZ) and differ from the SS export fluxes (Table 2 and Fig. 4a). For stations S2 (42.5° S , SAZ), L3 (44.9° S , SAF), S3 (47.5° S , PFZ), and S4 (51.9° S , SACCF), the NSS ^{234}Th flux is significantly lower than the SS flux and represents only between 15 % at 42.5° S (station S2) to 54 % at 44.9° S (station L3) of the latter. Such a difference indicates that surface export production was not at steady state over the time period separating the site occupations (15 to 21 days), partly due to variable total ^{234}Th activity. In this case, lower NSS fluxes support an increase of the total ^{234}Th activity in the surface ML ($\frac{dA_{\text{Th}}}{dt} > 0$) due to larger contribution of ^{234}Th in-growth from ^{238}U . By contrast, the situation is different at 55.2° S (stations L7, AZ) and at 57.6° S (station S5, WG). There the ^{234}Th fluxes evaluated using SS or NSS models show excellent agreement suggesting that surface ^{234}Th export has remained relatively constant over the period separating the two cruises (22 days).

(b) Mesopelagic ^{234}Th fluxes

Export fluxes of ^{234}Th at 600 m (called mesopelagic export flux here) are estimated for 8 stations for which upper 1000 m profiles of total ^{234}Th activities are available. These deep ^{234}Th fluxes are reported in Fig. 4b, as calculated using only the SS model since no initial ^{234}Th values are available for the mesopelagic zone. Negative fluxes of ^{234}Th (i.e., ^{234}Th excess over ^{238}U) for the 100–600 m depth interval correspond to a net accumulation of ^{234}Th and probably reflect a break-up or degradation of ^{234}Th -bearing particles within the mesopelagic layer due to remineralisation/disaggregation. As illustrated in Fig. 4b, the mesopelagic accumulation of ^{234}Th (i.e. negative fluxes) varies

BGD

9, 3423–3477, 2012

Late summer particulate organic carbon export

F. Planchon et al.

Title Page

Abstract

Introduction

Conclusions

References

Tables

Figures

◀

▶

◀

▶

Back

Close

Full Screen / Esc

Printer-friendly Version

Interactive Discussion



Late summer particulate organic carbon export

F. Planchon et al.

Title Page

Abstract

Introduction

Conclusions

References

Tables

Figures

◀

▶

◀

▶

Back

Close

Full Screen / Esc

Printer-friendly Version

Interactive Discussion

largely with latitude, ranging from $-458 \text{ dpm m}^{-2} \text{ d}^{-1}$ at 36.5° S (station S1, STZ) to $-3068 \text{ dpm m}^{-2} \text{ d}^{-1}$ at 47.5° S (station S3, PFZ). It is strongest in the PFZ and the SAZ (-1368 to $-3068 \text{ dpm m}^{-2} \text{ d}^{-1}$) and largely exceeds SS ^{234}Th export from the upper 100 m at 42.5° S (station S2, SAZ), 44.9° S (station L3, SAF) and 47.5° S (station S3, PFZ), resulting in negative total export fluxes from the upper 600 m. Smaller ^{234}Th accumulation rates (-554 to $-921 \text{ dpm m}^{-2} \text{ d}^{-1}$) are observed in the southern part of the BGH section. South of the PF, between 51.9° S (S4; SACCF) and 57.6° S (S5; WG), the mesopelagic accumulation of excess ^{234}Th is of similar magnitude, or smaller than the SS surface ^{234}Th export flux, but it consistently decreases (S4, SACCF, and L7, AZ) or cancels (S5) the total export flux of ^{234}Th at 600 m depth.

3.1.2 Particulate ^{234}Th and POC

Particulate ^{234}Th activities ($^{234}\text{Th}_p$) and POC concentrations for total suspended material (SPM) and for the two particle size classes ($>53 \mu\text{m}$ and $1 \gg 53 \mu\text{m}$) at super stations are presented in Fig. 5. High POC concentrations and $^{234}\text{Th}_p$ activities are observed in the upper mixed layer but decrease rapidly in the subsurface waters and remain essentially constant below 200 m. Surface POC and $^{234}\text{Th}_p$ activity of total SPM range from 0.46 to $3.60 \text{ } (\mu\text{mol L}^{-1})$ and from 0.28 to $0.99 \text{ } (\text{dpm L}^{-1})$, respectively. Highest total POC concentrations and $^{234}\text{Th}_p$ activities are observed in the SAZ (S2; 42.5° S) and in the PFZ (S3; 47.5° S). Lowest total POC and $^{234}\text{Th}_p$ values are encountered in the surface waters of the STZ (S1; 36.5° S) and the northern WG (S5; 57.6° S). From STZ (S1) to SACCF (S4), the $1 \gg 53 \mu\text{m}$ size fraction represents between 85 to 93 % of total POC and from 84 to 96 % of total $^{234}\text{Th}_p$. This situation changes south of the Sbdy (S5, 57.6° S) where 26 % of total POC and 37% of total $^{234}\text{Th}_p$ activity appears associated with large ($>53 \mu\text{m}$) particles.

3.2 POC to ^{234}Th ratios on particles

Profiles of $\text{POC}/^{234}\text{Th}_p$ ratios for the two particle size-fractions are plotted in Fig. 6. Measured $\text{POC}/^{234}\text{Th}_p$ ratios vary from 0.7 to $6.8\ \mu\text{mol dpm}^{-1}$ and from 0.8 to $16.3\ \mu\text{mol dpm}^{-1}$ in small ($1 \gg 53\ \mu\text{m}$) and large ($>53\ \mu\text{m}$) particles, respectively. For most stations the mixed layer $\text{POC}/^{234}\text{Th}$ ratios of the particles sizing $1 << 53\ \mu\text{m}$ are larger (S2, S3, S5) or similar (S1) compared with those for large ($>53\ \mu\text{m}$) particles. This is not the case at S4 (51.9°S ; SACCF), where surface $\text{POC}/^{234}\text{Th}_p$ ratios for $>53\ \mu\text{m}$ particles ($5.7\text{--}7.4\ \mu\text{mol dpm}^{-1}$) are about twice as large as for the $1 \gg 53\ \mu\text{m}$ particles ($2.9\text{--}3.6\ \mu\text{mol dpm}^{-1}$). Below the upper ML, $\text{POC}/^{234}\text{Th}_p$ ratios of small ($1 \gg 53\ \mu\text{m}$) particles in all cases decrease with depth to reach relatively constant values in the mesopelagic zone ($1.0\ \mu\text{mol dpm}^{-1}$ at S1, $1.4\ \mu\text{mol dpm}^{-1}$ at S2; $1.7\ \mu\text{mol dpm}^{-1}$ at S3; $2.8\ \mu\text{mol dpm}^{-1}$ at S4; $3.6\ \mu\text{mol dpm}^{-1}$ at S5). For large ($>53\ \mu\text{m}$) particles, $\text{POC}/^{234}\text{Th}_p$ ratios are much more variable in the mesopelagic zone (Fig. 6). A trend of decreasing $\text{POC}/^{234}\text{Th}_p$ ratios can be observed at S1 and S4 while ratios remain relatively unchanged, or even increase with depth at S3 and S2, respectively. At S3 the very large values (14.1 to $16.3\ \mu\text{mol dpm}^{-1}$) reported for the $>53\ \mu\text{m}$ particles between 400 and 500 m are likely due to zooplankton collected on the filter (revealed by visual inspection).

For estimating POC export fluxes, the $\text{POC}/^{234}\text{Th}_p$ ratio of sinking particles at the export depth has to be determined (Buesseler et al., 1992). As recommended by Buesseler et al. (2006), we consider the $\text{POC}/^{234}\text{Th}_p$ ratio of large ($>53\ \mu\text{m}$) particles as representative of sinking material leaving the upper ML. In this study and as illustrated in Fig. 6, no clear relationship exists between $\text{POC}/^{234}\text{Th}_p$ ratios of $>53\ \mu\text{m}$ particles and depth making it difficult to calculate this ratio for the exact 100 m depth horizon using a fitting function, such as for instance a power law (Jacquet et al., 2011). In order to take into account the observed $\text{POC}/^{234}\text{Th}_p$ variability below the export zone, we consider the average $\text{POC}/^{234}\text{Th}_p$ ratios between the basis of the ML and 300 m depth

BGD

9, 3423–3477, 2012

**Late summer
particulate organic
carbon export**

F. Planchon et al.

Title Page

Abstract

Introduction

Conclusions

References

Tables

Figures

◀

▶

◀

▶

Back

Close

Full Screen / Esc

Printer-friendly Version

Interactive Discussion



(Fig. 7). The smallest ratios are observed in the STZ (S1; $1.9 \pm 0.2 \mu\text{mol dpm}^{-1}$, $n = 3$) and the SAZ (S2; $1.7 \pm 0.2 \mu\text{mol dpm}^{-1}$, $n = 4$). South of the SAF, the $\text{POC}/^{234}\text{Th}_p$ ratio of sinking particles gradually increases from $3.0 \pm 0.2 \mu\text{mol dpm}^{-1}$ in the PFZ ($n = 2$; S3) to $5.6 \pm 1.3 \mu\text{mol dpm}^{-1}$ in the southern ACC ($n = 3$; S4) and $4.1 \pm 1.7 \mu\text{mol dpm}^{-1}$ in the WG ($n = 4$; S5). Such a southward increase of $\text{POC}/^{234}\text{Th}_p$ ratios of sinking particles was also observed in the SE-Pacific, between the SAZ and the Ross Sea for particles sizing $>70 \mu\text{m}$ (Buesseler et al., 2001).

To check the robustness of our averaging approach for evaluating $\text{POC}/^{234}\text{Th}$ ratios of sinking particles we also fitted power law functions to the vertical profiles of POC and $^{234}\text{Th}_p$ of the $>53 \mu\text{m}$ particle size fraction (Table 2). In this case, both, vertical profiles of POC and $^{234}\text{Th}_p$ appear well described using power law fits (R^2 ranging from 0.83 to 0.92 for both $>0.53 \mu\text{m}$ POC and $^{234}\text{Th}_p$). Fitted values for POC and $^{234}\text{Th}_p$ at 100 m depth are then used to deduce the $\text{POC}/^{234}\text{Th}_p$ ratio at 100 m (Table 2). Fitted $\text{POC}/^{234}\text{Th}$ ratios at 100 m are very similar to average ratios of $\text{POC}/^{234}\text{Th}_p$ between ML and 300 m (Fig. 7).

Though overall our $\text{POC}/^{234}\text{Th}_p$ ratios of sinking particles (Fig. 7) are of similar magnitude as those reported by others for the ACC, regional differences exist. For instance, $\text{POC}/^{234}\text{Th}_p$ ratios of sinking material in the PFZ (S3) and the WG (S5) are 1.5 to 1.8 times larger than those for the $>70 \mu\text{m}$ size fraction sampled at the same locations 18 to 22 days earlier (Rutgers van der Loeff et al., 2011). Our range of $\text{POC}/^{234}\text{Th}_p$ ratio for the $>53 \mu\text{m}$ fraction ($1.7\text{--}4.8 \mu\text{mol dpm}^{-1}$) is larger than the one reported by Copola et al. (2005) for the Indian sector of the ACC ($0.8\text{--}1.4 \mu\text{mol dpm}^{-1}$) but smaller than the ratios measured during bloom conditions in natural iron-fertilized settings close to Crozet ($5.5\text{--}10.8 \mu\text{mol dpm}^{-1}$; Morris et al., 2007) and Kerguelen island ($5.9\text{--}11 \mu\text{mol dpm}^{-1}$; Savoye et al., 2008). Our SAZ $\text{POC}/^{234}\text{Th}_p$ ratios for $>53 \mu\text{m}$ particles ($1.74 \pm 0.21 \mu\text{mol dpm}^{-1}$) are similar to those reported for the eastern SAZ, south of Tasmania by Jacquet et al. (2011; $2.06 \pm 0.30 \mu\text{mol dpm}^{-1}$ at 100 m) but smaller than for the western SAZ in the Australian sector (Jacquet et al., 2011; $3.93 \pm 0.77 \mu\text{mol dpm}^{-1}$

Late summer particulate organic carbon export

F. Planchon et al.

[Title Page](#)[Abstract](#)[Introduction](#)[Conclusions](#)[References](#)[Tables](#)[Figures](#)[◀](#)[▶](#)[◀](#)[▶](#)[Back](#)[Close](#)[Full Screen / Esc](#)[Printer-friendly Version](#)[Interactive Discussion](#)

at 100 m). For the PFZ, our $\text{POC}/^{234}\text{Th}_p$ ratio ($3.01 \pm 0.21 \mu\text{mol dpm}^{-1}$) is also smaller than the one observed in the PFZ during SAZ-Sense ($5.13 \pm 0.83 \mu\text{mol dpm}^{-1}$ at 100 m; Jacquet et al., 2011).

At “L” stations we did not deploy large volume in-situ pumps. Therefore, for stations located close to a biogeochemical boundary (L2-STF, L3-SAF, L6-PF, and L7-Sbdy), $\text{POC}/^{234}\text{Th}_p$ ratios were calculated by averaging the $\text{POC}/^{234}\text{Th}_p$ ratios measured in adjacent northern and southern zones (Table 3). For stations L4 and L5, located in the PFZ, we used the $\text{POC}/^{234}\text{Th}_p$ ratio obtained for S3 in the PFZ to calculate the POC flux.

3.3 ^{234}Th -derived carbon flux

3.3.1 Surface export production

Carbon export flux at 100 m (EP_{100}) is estimated by multiplying the NSS or SS export fluxes of ^{234}Th ($P_{234\text{Th}}$) at 100 m with the $\text{POC}/^{234}\text{Th}_p$ ratio of sinking particles:

$$P_{\text{POC}} = P_{234\text{Th}} \times \left(\frac{\text{POC}}{234\text{Th}} \right) \quad (6)$$

With P_{POC} in $\text{mmol m}^{-2} \text{d}^{-1}$, $P_{234\text{Th}}$ in $\text{dpm m}^{-2} \text{d}^{-1}$, and $\text{POC}/^{234}\text{Th}_p$ in mmol dpm^{-1} .

Overall EP_{100} ranges from 0.9 to 5.1 $\text{mmol m}^{-2} \text{d}^{-1}$ and from 0.3 to 4.9 $\text{mmol m}^{-2} \text{d}^{-1}$ based on the SS and NSS model, respectively (Fig. 8a; Table 3). The SS EP_{100} increases progressively from north to south. It remains low in the northern part of the transect, from 0.9 to 1.9 $\text{mmol m}^{-2} \text{d}^{-1}$ in the STZ (S1 and L2) and 1.7 $\text{mmol m}^{-2} \text{d}^{-1}$ in the SAZ. Further south, the SS EP_{100} increases gradually from 2.3 ± 0.7 to $3.5 \pm 0.4 \text{ mmol m}^{-2} \text{d}^{-1}$ (PFZ) to $4.7 \pm 2.6 \text{ mmol m}^{-2} \text{d}^{-1}$ (southern ACC, L6). South of the ACC in the AZ, SS EP_{100} reaches its maximal value ($5.1 \pm 2.1 \text{ mmol m}^{-2} \text{d}^{-1}$) and then decreases to $3.3 \pm 0.2 \text{ mmol m}^{-2} \text{d}^{-1}$ in the northern branch of the WG. NSS

Title Page

Abstract

Introduction

Conclusions

References

Tables

Figures

◀

▶

◀

▶

Back

Close

Full Screen / Esc

Printer-friendly Version

Interactive Discussion



EP₁₀₀ fluxes integrating the 15 to 22 day period preceding the BGH cruise also exhibit a latitudinal gradient but the variability is larger compared to the SS approach (Fig. 8a). The highest NSS EP₁₀₀ fluxes are observed in the AZ, south of the ACC ($4.9 \pm 3.2 \text{ mmol m}^{-2} \text{ d}^{-1}$) and in the WG ($3.1 \pm 1.3 \text{ mmol m}^{-2} \text{ d}^{-1}$), with values in close agreement with SS estimates. Within the ACC, from the SAZ to the SACCF, NSS EP₁₀₀ fluxes range from 0.3 ± 0.0 to $1.7 \pm 0.7 \text{ mmol m}^{-2} \text{ d}^{-1}$ and represent only 15 to 53 % of the SS export flux.

The POC export flux from 100 m compares well with values obtained for the same transect a few weeks earlier (Rutgers van der Loeff et al., 2011). The best agreement is found when comparing C export fluxes based on POC/²³⁴Th_p ratios for similar size fractions (>53 μm or >70 μm). The matching between POC export fluxes based on total SPM POC/²³⁴Th ratios (Fig. 8a) is less clear. Though values from both cruises can be similar (AZ, L7; northern WG, S5), for some areas important differences are noted (SAZ, S2; PFZ, S3; SACCF, S4). This discrepancy may result from the facts that (1) ²³⁴Th export fluxes are different due to non steady state conditions and (2) in the Rutgers van der Loeff et al. (2011) study POC/²³⁴Th_p ratios for total SPM are 1.4 to 1.9 times larger than our ratios for large particles (>53 μm) (Rutgers van der Loeff et al., 2011).

3.3.2 Mesopelagic carbon export flux

In order to estimate the POC flux attenuation between 100–600 m depth we multiplied the accumulation fluxes of excess ²³⁴Th obtained in mesopelagic waters (based on SS model calculations) with the POC/²³⁴Th_p ratios of sinking particles (Fig. 8b). Attenuation of the POC flux is indicated by negative flux values, which range from $-0.9 \pm 0.1 \text{ mmol m}^{-2} \text{ d}^{-1}$ (S1, STZ) to $-9.2 \pm 1.3 \text{ mmol m}^{-2} \text{ d}^{-1}$ (S3, PFZ) and vary quite widely with latitude. Mesopelagic attenuation is lowest in the STZ at 36.5° S ($-0.9 \text{ mmol m}^{-2} \text{ d}^{-1}$) but increases to $-2.5 \pm 0.4 \text{ mmol m}^{-2} \text{ d}^{-1}$ at 42.5° S in the SAZ (S2) and to $-2.8 \pm 0.8 \text{ mmol m}^{-2} \text{ d}^{-1}$ in the vicinity of the SAF, at 44.9° S. The highest POC

**Late summer
particulate organic
carbon export**

F. Planchon et al.

Title Page

Abstract

Introduction

Conclusions

References

Tables

Figures

◀

▶

◀

▶

Back

Close

Full Screen / Esc

Printer-friendly Version

Interactive Discussion



flux attenuation ($-9.2 \pm 0.4 \text{ mmol m}^{-2} \text{ d}^{-1}$) occurs in the central PFZ at 47.5° S (S3) but values decrease progressively southward to $-4.1 \pm 0.6 \text{ mmol m}^{-2} \text{ d}^{-1}$ at 49.0° S (PFZ), $-2.6 \pm 1.1 \text{ mmol m}^{-2} \text{ d}^{-1}$ at 51.9° S (SACCF) and to $-3.8 \pm 1.6 \text{ mmol m}^{-2} \text{ d}^{-1}$ at the southernmost station S5 in the northern WG.

This attenuation of the POC flux in mesopelagic waters leads to a significant decrease of the export from the upper 600 m (EP_{600}). As illustrated in Fig. 8b, EP_{600} fluxes remain positive only for stations S1, (STZ), S4 (southern ACC) and L7 (AZ), with deep POC export representing between 20 % (L7) and $\sim 50\%$ (S1 and S4) of POC export from the surface. At stations S2 (SAZ; 42.5° S), L3 (SAF; 44.9° S (L3), L5 (PFZ; 49.0° S) and S5 (WG; 57.6° S) surface export and mesopelagic attenuation of POC can be considered in balance within analytical uncertainties, thus indicating no deep POC export there. However, at S3 (PFZ; 47.5° S) mesopelagic attenuation significantly exceeds surface POC export (2.8 times). Such imbalance suggests that the SS assumption is invalid for modelling ^{234}Th activity at S3. Note that under NSS assumption this discrepancy would even be larger since NSS POC export is $<$ SS POC export (Fig. 8a). A similar discrepancy between surface export and subsurface remineralisation is reported by Savoye et al. (2004a) for the AZ and in the Seasonal Ice Zone (SIZ) of the Australian sector. A possible explanation for this observed imbalance may be the decoupling of surface and mesopelagic processes, due for instance to lateral advection of surface waters. The strong eastward surface current in the central ACC may have advected surface waters with lower ^{234}Th deficit and lower particle export relative to the signal captured at mesopelagic depth.

3.3.3 Ba_{xS} profiles

Surface waters are depleted in Ba_{xS} . Concentrations start to increase at the basis of the MLD where the density gradient gets steeper (Figs. 2 and 3b). The depth where the buildup of the meso- Ba_{xS} starts is shallow ($\sim 50 \text{ m}$) in the STZ and SAZ but then progressively increases in the ACC ($\sim 100 \text{ m}$) to shoal again slightly southward. This

BGD

9, 3423–3477, 2012

Late summer particulate organic carbon export

F. Planchon et al.

Title Page

Abstract

Introduction

Conclusions

References

Tables

Figures

◀

▶

◀

▶

Back

Close

Full Screen / Esc

Printer-friendly Version

Interactive Discussion



follows quite well the latitudinal variation of the MLD (Fig. 4a and Table 2). This is consistent with previous observations and supports the view that aggregates formed at the basis of the mixed layer are loci where micro-barites precipitate (Cardinal et al., 2005). The Ba_{xs} contents are usually maximal in the 200–400 m layer but high values exceeding 300 pM can extend down to 600–800 m (L3, SAF; L5, PFZ; S5, WG). The highest value for the whole transect is reached at station L3 (SAF) at 250 m (>1000 pM). Such high values have already been reported on the SAF and SAZ (Jacquet et al., 2005). This Ba_{xs} maximum is surrounded by values which remain high (>400 pM) over the 125–475 depth range.

Ba_{xs} contents are the lowest for the northernmost (STZ-SAZ) and the southernmost (SACCF-AZ-WG) parts of the BGH section. This spatial variability is also clearly expressed in the depth weighted average mesopelagic Ba_{xs} (meso- Ba_{xs}) contents (125–600 m; Table 4). Meso- Ba_{xs} is minimal at S1 (STZ; 168 pM) and maximal at L3 (SAF; 497 pM). The two PFZ stations have meso- Ba_{xs} contents exceeding 300 pM while all other stations have moderate meso- Ba_{xs} contents (235–277 pM). Such a trend with maximum meso- Ba_{xs} values around the PFZ and lower values northward and southward has already been observed earlier (Cardinal et al., 2005).

The variations of meso- Ba_{xs} compare rather well with the excess Th flux integrated over the 100–600 m depth layer (Fig. 9a). Excluding one outlier (S3-PFZ station which exhibits by far the highest excess Th flux) there is a significant relationship between these two geochemical parameters ($R^2 = 0.73$ $p = 0.015$, Fig. 8a).

4 Discussion

4.1 Steady-state vs. non steady-state surface export production

The ^{234}Th -based approach reveals a latitudinal gradient of POC export production in late summer (Fig. 8a). The overall picture shows that SS EP₁₀₀ gradually increases from low values in the STZ (L2; $0.9 \pm 0.2 \text{ mmol m}^{-2} \text{ d}^{-1}$) and the SAZ (S2;

BGD

9, 3423–3477, 2012

Late summer particulate organic carbon export

F. Planchon et al.

Title Page

Abstract

Introduction

Conclusions

References

Tables

Figures

◀

▶

◀

▶

Back

Close

Full Screen / Esc

Printer-friendly Version

Interactive Discussion



Late summer particulate organic carbon export

F. Planchon et al.

Title Page

Abstract

Introduction

Conclusions

References

Tables

Figures

◀

▶

◀

▶

Back

Close

Full Screen / Esc

Printer-friendly Version

Interactive Discussion



$1.7 \pm 0.3 \text{ mmol m}^{-2} \text{ d}^{-1}$) to higher export production rates observed from the PF (L6; $4.7 \pm 2.6 \text{ mmol m}^{-2} \text{ d}^{-1}$) to the SACCF (S4; $5.1 \pm 2.1 \text{ mmol m}^{-2} \text{ d}^{-1}$). This latitudinal gradient of POC flux is amplified when considering the NSS flux calculations (Fig. 8a and Table 3). For a time window of 15 to 22 days, the NSS model indicates an increasing EP_{100} from the SAZ (S2; $0.3 \pm 0.0 \text{ mmol m}^{-2} \text{ d}^{-1}$) to the SACCF (S4; $1.7 \pm 0.7 \text{ mmol m}^{-2} \text{ d}^{-1}$). NSS and SS EP_{100} values are similar further south in the AZ (L7; $4.9 \pm 3.2 \text{ mmol m}^{-2} \text{ d}^{-1}$) and the northern WG (S5; $3.1 \pm 1.3 \text{ mmol m}^{-2} \text{ d}^{-1}$). The observed discrepancy between SS and NSS EP_{100} fluxes for the northern and central zones of the BGH transect (i.e., from SAZ to the SACCF) indicates that surface POC export has been variable over time. Late austral summer period covered by the NSS model (late February to mid-March) seems to be characterized by low export intensity (0.3 to $1.7 \text{ mmol m}^{-2} \text{ d}^{-1}$). By contrast, higher EP_{100} values obtained with the SS model (1.7 to $3.9 \text{ mmol m}^{-2} \text{ d}^{-1}$) may indicate that a significant fraction of the export occurred earlier in the growth season. This finding is supported further by the ^{234}Th export fluxes (at 100 m) from the ANTXXIV cruise (Rutgers van der Loeff et al., 2011). In the latter study, 100 m ^{234}Th export fluxes between 42° S and 53° S range from 1006 ± 94 to $1670 \pm 103 \text{ dpm m}^{-2} \text{ d}^{-1}$, and are similar (42.5° S , S2) or as much as 69% higher (44.9° S , L3) than our estimates. This suggests that significant particle export occurred prior to the late summer period sampled during BGH, possibly related to the spring bloom (December) revealed by monthly means of remotely sensed Chl *a* distribution between 42° S to 50° S (Rutgers van der Loeff et al., 2011).

For the southernmost stations L7 and S5, we find a close agreement between NSS and SS EP_{100} (ratio of NSS to SS EP_{100} is 1.14 and 0.95 at L7 and S5, respectively). This suggests that POC export has occurred under steady state conditions with no important changes over time in ^{234}Th activity (and consequently on ^{234}Th fluxes) at least at the time scale of ^{234}Th ($t_{1/2} = 24 \text{ d}$). This is clearly the case at 55.2° S (AZ, L7) and 57.6° S (N-WG, S5), our SS ^{234}Th fluxes ($1072 \pm 120 \text{ dpm m}^{-2} \text{ d}^{-1}$ at L7 and $800 \pm 83 \text{ dpm m}^{-2} \text{ d}^{-1}$ at S5) are in close agreement with the ones estimated at the same locations 22 days earlier by Rutgers van der Loeff et al. (2011) who have reported

1058 ± 97 dpm m⁻² d⁻¹ at 54.3° S and 848 ± 106 dpm m⁻² d⁻¹ at 57.0° S. This feature indicates that export of ²³⁴Th-bearing particles occurred in the AZ and the N-WG during late summer and contributed to compensate the ²³⁴Th in-growth by ²³⁸U decay. This finding is further supported by the Fe distribution measured during both BGH and a preceding cruise ANTXXIV (Chever et al., 2010; Klunder et al., 2011). Surface dissolved Fe (DFe) concentrations exhibit a rapid drawdown over 21 days, decreasing from 0.33 nM at 55.0° S (station 119) and 0.34 nM at 56.0° S (station 122) (Klunder et al., 2011) to <0.1 nM at 55.2° S (station L7) and 0.14 nM at 57.6° S (station S5) (Chever et al., 2010). This fast assimilation of DFe (over 22 days) gives support for late summer phytoplanktonic production which may have triggered surface POC export.

4.1.1 POC/²³⁴Th_p ratio of sinking particles

The latitudinal trend of POC/²³⁴Th_p ratios (Fig. 7) suggests that sinking particles have variable properties, as depending on plankton community and/or particle dynamics. The increase of the POC/²³⁴Th_p ratio for the >53 μm fraction south of the PF would be consistent with larger particle volume to surface areas (V:SA), thus indicating an increasing contribution of larger cells to export (Buesseler et al., 2006). Indeed, the occurrence of high POC/²³⁴Th_p ratios is well documented for SO high latitude systems dominated by diatoms (Buesseler et al., 2001, 2003, 2005; Friedrich et Rutgers van der Loeff, 2002; Rutgers van der Loeff et al., 1997, 2002; Savoye et al., 2008). This relationship between high POC/²³⁴Th_p ratio and diatom abundance seems to hold true for the BGH transect. The latitudinal distribution of chloropigments reveals important changes in the phytoplanktonic community (see Joubert et al., 2011 and references therein). The oligotrophic conditions in the STZ and the low surface silicate levels (<5–10 μm) in the SAZ and the northern PFZ (Le Moigne et al., 2012) support a mixed phytoplanktonic community composed of dinoflagellates, chromophytes, nanoflagellates, and cyanobacteria, but result in low diatom abundances (fucoxanthin) (Le Moigne et al., 2012). It is likely that such a mixed community supports mainly the production of

BGD

9, 3423–3477, 2012

Late summer particulate organic carbon export

F. Planchon et al.

Title Page

Abstract

Introduction

Conclusions

References

Tables

Figures

◀

▶

◀

▶

Back

Close

Full Screen / Esc

Printer-friendly Version

Interactive Discussion



small particles consistent with low $\text{POC}/^{234}\text{Th}_p$ ratios in sinking particles (Buesseler et al., 2006). South of the PF (50.4°S), which marks the transition from oligotrophic to HNLC conditions with silicate-rich ($>10\ \mu\text{m}$) surface waters (Bown et al., 2011; Fripiat et al., 2011), diatom abundance progressively increases with latitude and reach a maximum at 57.6°S in the WG (S5). The size distribution of surface POC and $^{234}\text{Th}_p$ at this station contrasts with the ones at northern stations, with up to 26 % and 37 % of total POC and $^{234}\text{Th}_p$ associated with the $>53\ \mu\text{m}$ size fraction, respectively. This suggests the influence of larger diatom cells to the surface water particle population and consequently could explain the higher $\text{POC}/^{234}\text{Th}_p$ ratio observed in sinking material.

The surface water $\text{POC}/^{234}\text{Th}_p$ ratios of large and small particles differ between sites (see Fig. 6). At S1, surface $\text{POC}/^{234}\text{Th}_p$ ratios of fine and large particles are similar (4.7 and $3.7\ \mu\text{mol dpm}^{-1}$, respectively). At S2, S3, and S5, $\text{POC}/^{234}\text{Th}_p$ ratios increase with decreasing particle size by a factor 1.5 (S2) to 2.0 (S3). However, at S4, the large particle $\text{POC}/^{234}\text{Th}_p$ ratio exceeds the ratio in small particles by 2.1 times. Buesseler et al. (2006) report an increase of $\text{POC}/^{234}\text{Th}_p$ ratios with particle size for different oceanographic settings, including the SO. In our case only station S4 conforms to this pattern which fits the V:SA model, pointing to a dominant influence of increasing cell size on particle $\text{POC}/^{234}\text{Th}_p$ ratio. Decreasing or unchanging ratios with particle size, as observed at S1, S2, S3, and S5, must involve other controlling factors. Our results for the latter 4 stations are in good agreement with $\text{POC}/^{234}\text{Th}_p$ ratios obtained for three particle size classes ($1\text{--}10\ \mu\text{m}$, $10\text{--}50\ \mu\text{m}$, and $>50\ \mu\text{m}$) during the ANTXXIV cruise conducted along the same section as BGH 3 weeks earlier (Rutgers van der Loeff et al., 2011). Similar $\text{POC}/^{234}\text{Th}_p$ ratios for both particle size classes as observed in the STZ (S1) may be consistent with rapid aggregation of small particles into larger sinking ones, possibly reflecting the impact of TEP-producing phytoplankton species (Buesseler et al., 2006). On the other hand decreasing $\text{POC}/^{234}\text{Th}_p$ ratios with particle size, as observed for surface waters at S3 in the PFZ ($2.4\ \mu\text{mol dpm}^{-1}$; $1\text{--}53\ \mu\text{m}$ fraction), $5.0\ \mu\text{mol dpm}^{-1}$; $>53\ \mu\text{m}$ fraction) and to a lesser extent S2 (SAZ) and S5 (WG)

BGD

9, 3423–3477, 2012

**Late summer
particulate organic
carbon export**

F. Planchon et al.

Title Page

Abstract

Introduction

Conclusions

References

Tables

Figures

◀

▶

◀

▶

Back

Close

Full Screen / Esc

Printer-friendly Version

Interactive Discussion



(Fig. 6), may reflect preferential C loss relative to ^{234}Th during large particle generation. This may include C degradation and recycling in the surface as well as variable C assimilation rates between trophic levels, including production of fecal material by zooplankton (Buesseler et al., 2006).

4.2 Surface export and biological production

Chlorophyll *a*, POC and PON measurements reveal that phytoplankton abundance was highest in the STZ (L2) and in the SAZ (S2) in late summer 2008 (Joubert et al., 2011). To the south, algal biomass decreases progressively in the PFZ and reaches minimum values between the SACCF and the Sbdy. Particulate ^{234}Th determined at “Super” stations appears closely related to biomass distribution: the regression of surface POC concentration (obtained from in-situ pumps sampling) and particulate ^{234}Th activity of total SPM yields a correlation coefficient (R^2) of 0.911 ($n = 7$). This relationship is preserved ($R^2 : 0.808$, $n = 48$) when considering full water column data obtained from in-situ pumps samples. Although particulate ^{234}Th appears to mirror plankton abundance, surface export production (EP100 and EPML) does not display any relationship with algal biomass. In the STZ and in the SAZ, POC export fluxes are minimal, whereas in the low Chl *a* and POC area at S4 in the AZ, EP100 is highest (Fig. 8a).

Insights into the processes controlling surface POC export can be given by nitrogen uptake measurements carried out using ^{15}N -labelled nitrate, ammonium and urea (Joubert et al., 2011). Results obtained in that study indicate that the late summer oligotrophic conditions observed in the STZ support a phytoplanktonic community based on regenerated production with low f-ratio (0.2) and with nitrogen uptake being dominated by urea (70% of total N uptake). This regenerated-based community appears dominated by small size phytoplankton, 51% of Chl *a* is associated with picophytoplankton ($<2\ \mu\text{m}$), what is consistent with the low POC flux deduced from ^{234}Th in this zone ($0.9\text{--}1.8\ \text{mmol m}^{-2}\ \text{d}^{-1}$). To the south, the decrease of regenerated production documented by Joubert et al. (2011) and which is concurrent with a decreasing

BGD

9, 3423–3477, 2012

Late summer particulate organic carbon export

F. Planchon et al.

Title Page

Abstract

Introduction

Conclusions

References

Tables

Figures

◀

▶

◀

▶

Back

Close

Full Screen / Esc

Printer-friendly Version

Interactive Discussion



contribution of smaller sized phytoplanktonic, parallels the trend of increasing EP100 (Fig. 8a), indicating that enhanced nutrient recycling within the microbial loop appears to impact on POC export. Comparison between EP100 fluxes and urea uptake using a linear fitting function indicate a negative relationship (slope of -0.59) though the correlation is poor ($R^2 : 0.195$, $n = 10$), indicating other controlling factors are operating as well.

New production (NP) estimated from NO_3^- uptake rates and f-ratios offers a means to quantify the C export (Joubert et al., 2011). Although the approach relies on a number of underlying assumptions (steady state conditions; no nitrification in the euphotic layer; validity of Redfield stoichiometry to convert N uptake to C equivalents), new production represents potentially the amount of “exportable production” in the euphotic zone (Sambrotto and Mace, 2000). In Fig. 9, we compare NP deduced from nitrate uptake with SS EP100 (Fig. 9a) and with NSS EP100 (Fig. 9b) based on the ^{234}Th approach. It can be observed that POC export fluxes deduced from ^{234}Th represent between 6 and 56 % of NP for SS EP100 and between 1 and 19 % of NP for NSS EP100. As discussed by Henson et al. (2011) and Joubert et al. (2011) reasons for such discrepancy include a possible overestimation of f-ratio because of nitrification in the euphotic layer, the export of dissolved organic carbon and the fact that uptake of other reduced N species, such as amino acids, is usually not considered in the f-ratio approach. Also, differences in time and space scales covered by the NP and the ^{234}Th approaches can partly explain the observed discrepancies. Bearing in mind that NP represents the potential export of both dissolved and particulate material, lower POC export estimated using ^{234}Th approach tends to suggest that POC export efficiency is particularly low throughout the BGH transect. This is especially true for the SAZ (6%), the PFZ (13 to 21%), the AZ (7%) and the N-WG (18%) and to a lesser extent at the PF (29%) and at the SACCF (56%). When considering the survey period defined by the NSS model (14 to 22 days before the BGH cruise), efficiency of POC export is even lower and represents only between 1 % (SAZ) to 19 % (SACCF) of “total exportable fraction” based on NP. Although the true export efficiency (Export/production ratio or The ratio,

BGD

9, 3423–3477, 2012

Late summer particulate organic carbon export

F. Planchon et al.

Title Page

Abstract

Introduction

Conclusions

References

Tables

Figures

◀

▶

◀

▶

Back

Close

Full Screen / Esc

Printer-friendly Version

Interactive Discussion



as defined by Buesseler et al., 1998) has to be gauged against Net Primary Production (NPP) estimated from C uptake rates and which were not measured during BGH, the comparison between EP100 and NP may indicate that the biological C pump in the SE-Atlantic appears particularly inefficient (relative to nitrate uptake) in exporting C out of the euphotic zone during late summer.

4.3 Mesopelagic POC remineralisation

From the vertical distribution of excess ^{234}Th activities and Ba_{xS} profiles in mesopelagic waters (Fig. 2), it appears that the height of the water column where particle remineralisation/disaggregation water is most intense, strongly varies along the BGH transect. In the STZ (S1) and in the WG (S5) ^{234}Th accumulation is relatively shallow and peaks in the subsurface between 120 and 250 m. Evidence of shallow remineralisation has also been reported for the NW Pacific (Maiti et al., 2010), the Sargasso Sea, as associated with mesoscale eddies (Buesseler et al., 2008), and in the SO during the SOFEX experiment (Buesseler et al., 2005). From the SAZ (S2) to the SACCF (S4) the water column layer of excess ^{234}Th and Ba_{xS} is consistently broader. As shown in Fig. 2, ^{234}Th enrichments extend from below the upper mixed layer to 400 m in the SAZ (S2) and 1000 m in the SAF (L3). Such a thick layer of excess ^{234}Th is in line with previous studies carried out in different sectors of the SO, including the central Weddell Gyre (Usbeck et al., 2002), the Atlantic sector (Rutgers van der Loeff et al., 1997), and the Australian sector (Savoye et al., 2004a). It has also been reported for Ba_{xS} (Jacquet et al., 2008, 2011).

Although there is a general positive correlation between remineralisation fluxes as calculated from Ba_{xS} and ^{234}Th over the 100–600 m depth range, there also are differences. Indeed, two outliers corresponding to the maximum values of the Ba_{xS} -based (L3; SAF) and excess ^{234}Th based POC fluxes (station S3 at PFZ) do not fit the regression. Excluding these two values yields to a correlation coefficient $R^2 = 0.73$ (Fig. 10b). A closer look at the data indicates that at some stations maxima of Ba_{xS} occur at

BGD

9, 3423–3477, 2012

Late summer particulate organic carbon export

F. Planchon et al.

Title Page

Abstract

Introduction

Conclusions

References

Tables

Figures

◀

▶

◀

▶

Back

Close

Full Screen / Esc

Printer-friendly Version

Interactive Discussion



different depths than ^{234}Th excess (Fig. 2). For instance, at L3 (SAF) ^{234}Th excess is highest around 150 m, whereas Ba_{XS} exhibits a sharp peak of 1079 pM at 250 m. In the central PFZ (S3) where remineralisation calculated from ^{234}Th is particularly strong, high Ba_{XS} concentrations occur between 250 and 500 m, below the maximum of ^{234}Th excess (between 120 m to 400 m). Such differences indicate that the break-up of ^{234}Th -bearing particles is not exactly overlapping with the release of Ba_{XS} rich particles from the aggregates and micro-environments in which they originally formed. This likely reflects differences in carrier particle size and compositions. It should also be kept in mind that both proxies have limitations inherent to the conversion from Ba_{XS} or ^{234}Th into carbon fluxes. It is quite striking to see that the correlation meso- Ba_{XS} vs. ^{234}Th fluxes for the 100–600 m depth interval (Fig. 9a) is indeed better (has only one outlier) compared to the regression of the corresponding fluxes. It is likely that a significant part of the discrepancies between the two proxies comes from the assumptions made to calculate C fluxes. For Ba_{XS} this is mainly based on the use of an empiric algorithm, for ^{234}Th , the main uncertainty probably resides in the choice of the $\text{POC}/^{234}\text{Th}_\rho$ ratio of remineralised material.

Despite such differences, remineralisation fluxes calculated using the Ba_{XS} and excess ^{234}Th proxy approaches are of similar magnitude (Fig. 11). We also note that remineralisation fluxes of carbon (C_{respired}) are of the same order of magnitude as the fluxes of POC sinking from the surface, giving further support to the idea that a large fraction of surface export production is strongly attenuated in the mesopelagic zone. However, some differences exist between the two proxies. Close to the SAF (44.9° S), C_{respired} from Ba_{XS} data is ~ 2 times higher than excess ^{234}Th -based estimates, suggesting that some C remineralisation took place earlier in the season and was not integrated by the excess ^{234}Th approach. By contrast, in the PFZ (47.5° S), POC remineralisation deduced from excess ^{234}Th appears 5 times higher than C_{respired} deduced from Ba_{XS} . It is possible that in this case we see an effect due to physicochemical fragmentation of sinking aggregates as well particle input associated with by zooplankton

Late summer particulate organic carbon export

F. Planchon et al.

[Title Page](#)[Abstract](#)[Introduction](#)[Conclusions](#)[References](#)[Tables](#)[Figures](#)[◀](#)[▶](#)[◀](#)[▶](#)[Back](#)[Close](#)[Full Screen / Esc](#)[Printer-friendly Version](#)[Interactive Discussion](#)

migration. These would affect the total ^{234}Th distribution and would not necessarily be paralleled by increased bacterial remineralisation of sinking POC, affecting the Ba_{XS} content.

Overall however, these results confirm that the PFZ (and SAF) is a zone of very efficient mesopelagic remineralisation. Remineralisation rates often exceed export rates from the surface, probably reflecting the fact that the BGH cruise took place in late summer at a time where primary production is decreasing, i.e. when export was already relatively low. It is possible that mesopelagic remineralisation proceeds on particles which were formed earlier in the season and were associated with larger export fluxes. Such a trend toward higher remineralisation rates during the progress of the growth season is a feature that has also been reported in the Southern Ocean (Cardinal et al., 2005; Jacquet et al., 2011).

The fate of the exported POC when transiting through the mesopelagic to bathypelagic zone (>1000 m depth) determines longer term sequestration of POC. In Fig. 12, POC sequestration efficiency to depths >600 m (here defined as the fraction of the exportable production reaching depths >600 m) is explored for the BGH area by considering the ratio of POC flux at 100 m depth over new production estimated from nitrate uptake (EP100/NP) versus the transfer efficiency through the mesopelagic, defined by the ratio of POC flux at 600 m (i.e. EP600 = EP100 – remineralisation flux) relative to the POC flux at 100 m (EP600/EP100) (Jacquet et al., 2011). Sequestration efficiency appears negligible in the SAZ, the PFZ and the N-WG although the export production from the surface can represent up to ~20 % of NP in the PFZ, <20 % in the N-WG, <15 % at the SAF and <5 % in the SAZ. The AZ and the STZ both have relatively low fractions of NP that are exported below 100 m depth (7 % for the AZ and 29 % for the STZ) but they significantly differ in the fraction of exported POC from the surface (EP100) that reaches the bathypelagic zone below 600 m depth (20 % for the AZ and ~50% for the STZ). Sequestration efficiency is higher in the STZ (15 %) than in the AZ where only ~1 % of NP is exported below 600 m depth. Nevertheless, the highest sequestration efficiency is observed at the SACCF, there more than 25 % of NP is

Late summer particulate organic carbon export

F. Planchon et al.

[Title Page](#)[Abstract](#)[Introduction](#)[Conclusions](#)[References](#)[Tables](#)[Figures](#)[◀](#)[▶](#)[◀](#)[▶](#)[Back](#)[Close](#)[Full Screen / Esc](#)[Printer-friendly Version](#)[Interactive Discussion](#)

exported to the depth >600 m depth due to lower attenuation of the POC flux in the 100–600 m depth interval.

5 Conclusions

In this Southern Ocean study the distribution of short-lived ^{234}Th and biogenic particulate Ba (Ba_{XS}) are combined to document late summer export of POC from the surface and its fate in the mesopelagic zone.

Steady state modelling of ^{234}Th deficit predicts lowest export production in the STZ and the SAZ where highest levels of biomass are observed. To the south, across the PFZ into the Southern ACC, export production increases progressively, in line with substantial broadening of the surface mixed layer and increasing POC to ^{234}Th ratios of sinking particles. South of the ACC, the AZ and the northern branch of the Weddell Gyre we observed a slight decrease in POC export, though values still exceed those for the STZ and the SAZ. This could partly result from a greater abundance of large diatoms in sinking material. Non steady state modelling of the ^{234}Th flux allowed to constrain export production over a period of 2 to 3 weeks prior to BGH expedition. For the area between SAZ and SACCF the non steady state model revealed significantly lower POC export compared to the steady state calculation, suggesting that late summer conditions with low silicate and iron levels, combined with predominance of regenerated production could be factors limiting export. In contrast, further south, in the AZ and the northern Weddell Gyre the two modelling approaches (non steady state and steady state) yield similar values for POC export, indicating export production in this low productivity and high nutrient area remained relatively constant over the season. Although ^{234}Th -based export fluxes and new production estimates exhibit a similar increasing trend southward, ^{234}Th based fluxes are consistently lower. Considering that new production represents the “total potentially exportable fraction” of organic C, the discrepancy observed between the two proxies may indicate that surface POC export efficiency is particularly low in late summer.

Late summer particulate organic carbon export

F. Planchon et al.

Title Page

Abstract

Introduction

Conclusions

References

Tables

Figures

◀

▶

◀

▶

Back

Close

Full Screen / Esc

Printer-friendly Version

Interactive Discussion



Below the export zone in the mesopelagic layer, excess ^{234}Th activities as well as accumulation of particulate biogenic Ba, provide strong evidence for significant though variable degrees of POC remineralisation. The attenuation of sinking particles appears particularly intense across the ACC, between the STF and the SACCF. While remineralisation in the SAZ, the AZ and the N-WG essentially occurs between subsurface and 400 m, it extends much deeper for the region bounded by SAF and PF leading to highest attenuations of export being located there. Although some differences exist between the two independent proxies, excess ^{234}Th and meso- Ba_{XS} yield similar estimates of POC remineralisation. When compared to export production we find that remineralisation of POC in the twilight zone is particularly efficient in the studied area thereby controlling longer term bathypelagic POC sequestration.

Supplementary material related to this article is available online at:
<http://www.biogeosciences-discuss.net/9/3423/2012/bgd-9-3423-2012-supplement.pdf>

Acknowledgements. The BONUS-GoodHope cruise is part of the IPY ICED and GEOTRACES programmes. We are grateful to co-chief scientists Sabrina Speich and Marie Boyé, the French Polar Institute, IPEV (Institut Paul Emile Victor) and the captain and crew of R/V *Marie Dufresne* for their assistance during cruise preparation and operations at sea. We are also grateful to Michael Korntheuer for state of the art beta counter maintenance, Jacques Navez, Laurence Monnin, and Nouredine Dakhani for helpful laboratory assistance. This work was supported by the Federal Belgian Science Policy Office (BELSPO) under the Science for Sustainable Development (SDD) program (Integrated Study of Southern Ocean Biogeochemistry and Climate Interaction in the Anthropocene BELCANTO contracts EV/37/7C, EV/03/7A, SD/CA/03A).

BGD

9, 3423–3477, 2012

Late summer particulate organic carbon export

F. Planchon et al.

Title Page

Abstract

Introduction

Conclusions

References

Tables

Figures

◀

▶

◀

▶

Back

Close

Full Screen / Esc

Printer-friendly Version

Interactive Discussion



References

- Bowie, A. R., Brian Griffiths, F., Dehairs, F. and Trull, T. W.: Oceanography of the subantarctic and Polar Frontal Zones south of Australia during summer: Setting for the SAZ-Sense study, *Deep Sea Res. Pt. II*, 58, 2059–2070, 2011.
- 5 Bown, J., Boye, M., Baker, A., Duvieilbourg, E., Lacan, F., Le Moigne, F., Planchon, F., Speich, S. and Nelson, D. M.: The biogeochemical cycle of dissolved cobalt in the Atlantic and the Southern Ocean south off the coast of South Africa, *Mar. Chem.*, 126, 193–206, 2011.
- Boyd, P. W.: The role of iron in the biogeochemistry of the Southern Ocean and equatorial Pacific: a comparison of in situ iron enrichments, *Deep Sea Res. Pt. II*, 49, 1803–1821, 10 2002.
- Boyd, P. W. and Trull, T. W.: Understanding the export of biogenic particles in oceanic waters: Is there consensus?, *Prog. Oceanogr.*, 72, 276–312, 2007.
- Buesseler, K. O.: The decoupling of production and particulate export in the surface ocean, *Global Biogeochem. Cycles*, 12(2), 297–310, 1998.
- 15 Buesseler, K. O., Antia, A. N., Min Chen, Fowler, S. W., Gardner, W. D., Gustafsson, O., Harada, K., Michaels, A. F., van der Loeff, M. R., Sarin, M., Steinberg, D. K., et al.: An assessment of the use of sediment traps for estimating upper ocean particle fluxes., *J. Mar. Res.*, 65(3), 345–416, 2007.
- Buesseler, K. O., Bacon, M. P., Kirk Cochran, J. and Livingston, H. D.: Carbon and nitrogen 20 export during the JGOFS North Atlantic Bloom experiment estimated from ^{234}Th : ^{238}U disequilibria, *Deep Sea Res. Pt. A*, 39, 1115–1137, 1992.
- Buesseler, K. O., Ball, L., Andrews, J., Cochran, J. K., Hirschberg, D. J., Bacon, M. P., Fleer, A. and Brzezinski, M.: Upper ocean export of particulate organic carbon and biogenic silica in the Southern Ocean along 170°W , *Deep Sea Res. Pt. II*, 48, 4275–4297, 2001.
- 25 Buesseler, K. O., Barber, R. T., Dickson, M.-L., Hiscock, M. R., Moore, J. K. and Sambrotto, R.: The effect of marginal ice-edge dynamics on production and export in the Southern Ocean along 170°W , *Deep Sea Res. Pt. II*, 50, 579–603, 2003.
- Buesseler, K. O., Andrews, J., Pike, S. M., Charette, M. A., Goldson, L. E., Brzezinski, M. A. and Lance, V. P.: Particle export during the Southern Ocean Iron Experiment (SOFEX), *Limnol. Oceanogr.*, 50, 311–327, 2005.
- 30 Buesseler, K. O., Benitez-Nelson, C. R., Moran, S. B., Burd, A., Charette, M., Cochran, J. K., Coppola, L., Fisher, N. S., Fowler, S. W., Gardner, W. D., Guo, L. D., et al.: An assessment

BGD

9, 3423–3477, 2012

Late summer particulate organic carbon export

F. Planchon et al.

Title Page

Abstract

Introduction

Conclusions

References

Tables

Figures

◀

▶

◀

▶

Back

Close

Full Screen / Esc

Printer-friendly Version

Interactive Discussion



Late summer particulate organic carbon export

F. Planchon et al.

Title Page

Abstract

Introduction

Conclusions

References

Tables

Figures

◀

▶

◀

▶

Back

Close

Full Screen / Esc

Printer-friendly Version

Interactive Discussion



of particulate organic carbon to thorium-234 ratios in the ocean and their impact on the application of ^{234}Th as a POC flux proxy, *Mar. Chem.*, 100, 213–233, 2006.

Buesseler, K. O., Lamborg, C., Cai, P., Escoube, R., Johnson, R., Pike, S., Masque, P., McGillicuddy, D. and Verdeny, E.: Particle fluxes associated with mesoscale eddies in the Sargasso Sea, *Deep Sea Res. Pt. II*, 55, 1426–1444, 2008.

Buesseler, K. O., Pike, S., Maiti, K., Lamborg, C. H., Siegel, D. A. and Trull, T. W.: Thorium-234 as a tracer of spatial, temporal and vertical variability in particle flux in the North Pacific, *Deep Sea Res. Pt. I*, 56, 1143–1167, 2009.

Cardinal, D., Dehairs, F., Cattaldo, T. and André, L.: Geochemistry of suspended particles in the Subantarctic and Polar Frontal Zones south of Australia: Constraints on export and advection processes, *J. Geophys. Res.*, 106, 31637–31656, doi:10.1029/2000JC000251, 2001.

Cardinal, D., Savoye, N., Trull, T. W., André, L., Kopczynska, E. E. and Dehairs, F.: Variations of carbon remineralisation in the Southern Ocean illustrated by the Baxs proxy, *Deep Sea Res. Pt. I*, 52, 355–370, 2005.

Chen, J. H., Lawrence Edwards, R. and Wasserburg, G. J.: ^{238}U , ^{234}U and ^{232}Th in seawater, *Earth Planet. Sci. Lett.*, 80, 241–251, 1986.

Chever, F., Bucciarelli, E., Sarthou, G., Speich, S., Arhan, M., Penven, P. and Tagliabue, A.: Physical speciation of iron in the Atlantic sector of the Southern Ocean along a transect from the subtropical domain to the Weddell Sea Gyre, *J. Geophys. Res.*, 115, C10059, doi:10.1029/2009JC005880, 2010.

Cochran, J. K. and Masqué, P.: Short-lived U/Th series radionuclides in the ocean: tracers for scavenging rates, export fluxes and particle dynamics, *Uranium-series geochemistry*, 52, 461–492, 2003.

Coppola, L., Roy-Barman, M., Mulsow, S., Povinec, P. and Jeandel, C.: Low particulate organic carbon export in the frontal zone of the Southern Ocean (Indian sector) revealed by ^{234}Th , *Deep Sea Res. Pt. I*, 52, 51–68, 2005.

de Boer, A. M., Watson, A. J., Edwards, N. R., and Oliver, K. I. C.: A multi-variable box model approach to the soft tissue carbon pump, *Clim. Past*, 6, 827–841, doi:10.5194/cp-6-827-2010, 2010.

Dehairs, F., Chesselet, R. and Jedwab, J.: Discrete suspended particles of barite and the barium cycle in the open ocean, *Earth Planet. Sci. Lett.*, 49, 528–550, 1980.

Dehairs, F., Jacquet, S., Savoye, N., Van Mooy, B. A. S., Buesseler, K. O., Bishop, J. K. B., Lamborg, C. H., Elskens, M., Baeyens, W., Boyd, P. W., Casciotti, K. L., et al.: Barium in twilight

Late summer particulate organic carbon export

F. Planchon et al.

[Title Page](#)
[Abstract](#)
[Introduction](#)
[Conclusions](#)
[References](#)
[Tables](#)
[Figures](#)
[Back](#)
[Close](#)
[Full Screen / Esc](#)
[Printer-friendly Version](#)
[Interactive Discussion](#)


zone suspended matter as a potential proxy for particulate organic carbon remineralization: Results for the North Pacific, *Deep Sea Res. Pt. II*, 55, 1673–1683, 2008.

Dehairs, F., Shopova, D., Ober, S., Veth, C. and Goeyens, L.: Particulate barium stocks and oxygen consumption in the Southern Ocean mesopelagic water column during spring and early summer: relationship with export production, *Deep Sea Res. Pt. II*, 44(1-2), 497–516, 1997.

Friedrich, J. and Rutgers van der Loeff, M. M.: A two-tracer (^{210}Po - ^{234}Th) approach to distinguish organic carbon and biogenic silica export flux in the Antarctic Circumpolar Current, *Deep Sea Res. Pt. I*, 49, 101–120, 2002.

Fripiat, F., Cavagna, A.-J., Dehairs, F., Speich, S., André, L. and Cardinal, D.: Silicon pool dynamics and biogenic silica export in the Southern Ocean inferred from Si-isotopes, *Ocean Sci.*, 7(5), 533–547, 2011.

Ganeshram, R. S., François, R., Commeau, J. and Brown-Leger, S. L.: An experimental investigation of barite formation in seawater, *Geochim. Cosmochim. Acta*, 67, 2599–2605, 2003.

Gladyshev, S., Arhan, M., Sokov, A. and Speich, S.: A hydrographic section from South Africa to the southern limit of the Antarctic Circumpolar Current at the Greenwich meridian, *Deep Sea Res. Pt. I*, 55, 1284–1303, 2008.

Gruber, N., Gloor, M., Mikaloff Fletcher, S. E., Doney, S. C., Dutkiewicz, S., Follows, M. J., Gerber, M., Jacobson, A. R., Joos, F., Lindsay, K., Menemenlis, D. et al.: Oceanic sources, sinks, and transport of atmospheric CO_2 , *Global Biogeochem. Cycles*, 23, GB1005, 2009.

Henson, S. A., Sanders R., Madsen E., Morris P. J., Le Moigne F. and Quartly G. D.: A reduced estimate of the strength of the ocean's biological carbon pump, *Geophys. Res. Lett.*, 38, L04606, doi:10.1029/2011GL046735, 2011.

Jacquet, S. H. M., Dehairs, F., Cardinal, D., Navez, J. and Delille, B.: Barium distribution across the Southern Ocean frontal system in the Crozet-Kerguelen Basin, *Mar. Chem.*, 95, 149–162, 2005.

Jacquet, S. H. M., Dehairs, F., Dumont, I., Becquevort, S., Cavagna, A.-J. and Cardinal, D.: Twilight zone organic carbon remineralization in the Polar Front Zone and Subantarctic Zone south of Tasmania, *Deep Sea Res. Pt. II*, 58, 2222–2234, 2011.

Jacquet, S. H. M., Dehairs, F., Savoye, N., Obernosterer, I., Christaki, U., Monnin, C. and Cardinal, D.: Mesopelagic organic carbon remineralization in the Kerguelen Plateau region tracked by biogenic particulate Ba, *Deep Sea Res. Pt. II*, 55, 868–879, 2008.

Joubert, W. R., Thomalla, S. J., Waldron, H. N., Lucas, M. I., Boye, M., Le Moigne, F. A. C.,

**Late summer
particulate organic
carbon export**F. Planchon et al.

[Title Page](#)[Abstract](#)[Introduction](#)[Conclusions](#)[References](#)[Tables](#)[Figures](#)[◀](#)[▶](#)[◀](#)[▶](#)[Back](#)[Close](#)[Full Screen / Esc](#)[Printer-friendly Version](#)[Interactive Discussion](#)

Planchon, F. and Speich, S.: Nitrogen uptake by phytoplankton in the Atlantic sector of the Southern Ocean during late austral summer, *Biogeosciences*, 8, 2947–2959, 2011, <http://www.biogeosciences.net/8/2947/2011/>.

Klunder, M. B., Laan, P., Middag, R., De Baar, H. J. W. and Ooijen, J. v.: Dissolved iron in the Southern Ocean (Atlantic sector), *Deep Sea Res. Pt. II*, 58, 2678–2694, 2011.

Maiti, K., Benitez-Nelson, C. R. and Buesseler, K. O.: Insights into particle formation and remineralization using the short-lived radionuclide, Thorium-234, *Geophys. Res. Lett.*, 37, L15608, doi:10.1029/2010GL044063, 2010.

Martin, J. H., Knauer, G. A., Karl, D. M. and Broenkow, W. W.: VERTEX: carbon cycling in the northeast Pacific, *Deep Sea Res. Pt. A*, 34, 267–285, 1987.

McNeil, B. I., Metzl, N., Key, R. M., Matear, R. J. and Corbiere, A.: An empirical estimate of the Southern Ocean air-sea CO₂ flux, *Global Biogeochem. Cycles*, 21, GB3011, 2007.

McNeil, B. I. and Tilbrook, B.: A seasonal carbon budget for the sub-Antarctic Ocean, South of Australia, *Mar. Chem.*, 115, 196–210, 2009.

Le Moigne, F. A. C., Boye, M., Masson, A., Corvaisier, R., Grosstefan, E., Guéneugues, A., Pondaven, P. and Nelson, D.: Biogeochemical features of the subtropical southeastern Atlantic and the Southern Ocean south off South Africa during the austral summer of the International Polar Year, *Biogeosciences Discussion*, in prep., 2012.

Monnin, C. and Cividini, D.: The saturation state of the world's ocean with respect to (Ba,Sr)SO₄ solid solutions, *Geochim. Cosmochim. Acta*, 70, 3290–3298, 2006.

Monnin, C., Jeandel, C., Cattaldo, T. and Dehairs, F.: The marine barite saturation state of the world's oceans, *Mar. Chem.*, 65(3-4), 253–261, 1999.

Morris, P. J., Sanders, R., Turnewitsch, R. and Thomalla, S.: 234Th-derived particulate organic carbon export from an island-induced phytoplankton bloom in the Southern Ocean, *Deep Sea Res. Pt. II*, 54, 2208–2232, 2007.

Nelson, D. M., Anderson, R. F., Barber, R. T., Brzezinski, M. A., Buesseler, K. O., Chase, Z., Collier, R. W., Dickson, M.-L., François, R., Hiscock, M. R., Honjo, S., et al.: Vertical budgets for organic carbon and biogenic silica in the Pacific sector of the Southern Ocean, 1996–1998, *Deep Sea Res. Pt. II*, 49, 1645–1674, 2002.

Pates, J. M. and Muir, G. K. P.: U-salinity relationships in the Mediterranean: Implications for 234Th:238U particle flux studies, *Mar. Chem.*, 106, 530–545, 2007.

Pike, S. M., Buesseler, K. O., Andrews, J. and Savoye, N.: Quantification of 234Th recovery in small volume sea water samples by inductively coupled plasma-mass spectrometry, *J.*

**Late summer
particulate organic
carbon export**F. Planchon et al.

[Title Page](#)[Abstract](#)[Introduction](#)[Conclusions](#)[References](#)[Tables](#)[Figures](#)[◀](#)[▶](#)[◀](#)[▶](#)[Back](#)[Close](#)[Full Screen / Esc](#)[Printer-friendly Version](#)[Interactive Discussion](#)

Radioanal. Nucl. Ch., 263, 355–360, 2005.

Pondaven, P., Ruiz-Pino, D., Fravallo, C., Tréguer, P. and Jeandel, C.: Interannual variability of Si and N cycles at the time-series station KERFIX between 1990 and 1995 – a 1-D modelling study, *Deep Sea Res. Pt. I*, 47, 223–257, 2000.

5 Rutgers van der Loeff, M. M., Friedrich, J. and Bathmann, U. V.: Carbon export during the Spring Bloom at the Antarctic Polar Front, determined with the natural tracer ^{234}Th , *Deep Sea Res. Pt. II*, 44, 457–478, 1997.

Rutgers van der Loeff, M. M., Buesseler, K., Bathmann, U., Hense, I. and Andrews, J.: Comparison of carbon and opal export rates between summer and spring bloom periods in the region of the Antarctic Polar Front, SE Atlantic, *Deep Sea Res. Pt. II*, 49, 3849–3869, 2002.

10 Rutgers van der Loeff, M., Cai, P. H., Stimac, I., Bracher, A., Middag, R., Klunder, M. B. and van Heuven, S. M. A. C.: ^{234}Th in surface waters: distribution of particle export flux across the Antarctic Circumpolar Current and in the Weddell Sea during the GEOTRACES expedition ZERO and DRAKE, *Deep Sea Res. Pt. II*, 58, 2749–2766, 2011.

15 Sambrotto, R. N. and Mace, B. J.: Coupling of biological and physical regimes across the Antarctic Polar Front as reflected by nitrogen production and recycling. *Deep Sea Res. Pt. II*, 47, 3339–3367, 2000.

Sarmiento, J. L., Gruber, N., Brzezinski, M. A., and Dunne, J. P.: High-latitude controls of thermocline nutrients and low latitude biological productivity, *Nature*, 427, 56–60, 2004.

20 Savoye, N., Benitez-Nelson, C., Burd, A. B., Cochran, J. K., Charette, M., Buesseler, K. O., Jackson, G. A., Roy-Barman, M., Schmidt, S. and Elskens, M.: ^{234}Th sorption and export models in the water column: A review, *Mar. Chem.*, 100, 234–249, 2006.

Savoye, N., Buesseler, K. O., Cardinal, D. and Dehairs, F.: ^{234}Th deficit and excess in the Southern Ocean during spring 2001: Particle export and remineralization, *Geophys. Res. Lett.*, 31, L12301, doi:10.1029/2004GL019744, 2004a.

25 Savoye, N., Dehairs, F., Elskens, M., Cardinal, D., Kopczynska, E. E., Trull, T. W., Wright, S., Baeyens, W. and Griffiths, F. B.: Regional variation of spring N-uptake and new production in the Southern Ocean, *Geophys. Res. Lett.*, 31, L03301, doi:10.1029/2003GL018946, 2004b.

30 Savoye, N., Trull, T. W., Jacquet, S. H. M., Navez, J. and Dehairs, F.: ^{234}Th -based export fluxes during a natural iron fertilization experiment in the Southern Ocean (KEOPS), *Deep Sea Res. Pt. II*, 55, 841–855, 2008.

Shopova, D., Dehairs, F. and Baeyens, W.: A simple model of biogeochemical element distribution in the oceanic water column, *J. Marine Syst.*, 6, 331–344, 1995.

**Late summer
particulate organic
carbon export**F. Planchon et al.

[Title Page](#)[Abstract](#)[Introduction](#)[Conclusions](#)[References](#)[Tables](#)[Figures](#)[◀](#)[▶](#)[◀](#)[▶](#)[Back](#)[Close](#)[Full Screen / Esc](#)[Printer-friendly Version](#)[Interactive Discussion](#)

- Sigman, D. M. and Boyle, E. A.: Glacial/interglacial variations in atmospheric carbon dioxide., *Nature*, 407(6806), 859, 2000.
- Sternberg, E., Jeandel, C., Robin, E. and Souhaut, M.: Seasonal cycle of suspended barite in the mediterranean sea, *Geochim. Cosmochim. Acta*, 72, 4020–4034, 2008.
- 5 Takahashi, T., Sutherland, S. C., Wanninkhof, R., Sweeney, C., Feely, R. A., Chipman, D. W., Hales, B., Friederich, G., Chavez, F., Sabine, C., Watson, A., et al.: Climatological mean and decadal change in surface ocean pCO₂, and net sea-air CO₂ flux over the global oceans, *Deep Sea Res. Pt. II*, 56, 554–577, 2009.
- Taylor, S. R. and McLennan, S. M.: *The Continental Crust: its Composition and Evolution*, Blackwell Scientific Publications., 1985.
- 10 Trull, T. W., Bray, S. G., Buesseler, K. O., Lamborg, C. H., Manganini, S., Moy, C. and Valdes, J.: In situ measurement of mesopelagic particle sinking rates and the control of carbon transfer to the ocean interior during the Vertical Flux in the Global Ocean (VERTIGO) voyages in the North Pacific, *Deep Sea Res. Pt. II*, 55, 1684–1695, 2008.
- 15 Trull, T. W., Bray, S. G., Manganini, S. J., Honjo, S. and François, R.: Moored sediment trap measurements of carbon export in the Subantarctic and Polar Frontal Zones of the Southern Ocean, south of Australia, *J. Geophys. Res.*, 106, 31489–31509, doi:10.1029/2000JC000308, 2001.
- Usbeck, R., Rutgers van der Loeff, M., Hoppema, M. and Schlitzer, R.: Shallow remineralization in the Weddell Gyre, *Geochem. Geophys. Geosyst.*, 3, 1008, doi:10.1029/2001GC000182, 2002.
- 20 van Beek, P., Sternberg, E., Reyss, J.-L., Souhaut, M., Robin, E. and Jeandel, C.: 228Ra/226Ra and 226Ra/Ba ratios in the Western Mediterranean Sea: Barite formation and transport in the water column, *Geochim. Cosmochim. Acta*, 73, 4720–4737, 2009.

Late summer
particulate organic
carbon export

F. Planchon et al.

Table 1. ^{234}Th export fluxes ($\text{dpm m}^{-2} \text{d}^{-1}$) along the BGH transect calculated using Steady-State and Non Steady State models. Uncertainty associated with ^{234}Th flux is at 95 % confidence interval (2σ).

Station	Lat	Zone	Sampling date	ML depth ^a (m)	Steady State Model		non Steady State Model				
					^{234}Th export flux		1st Visit (Cruise ANTXXIV/3)		^{234}Th export flux		
					at 100 m ($\text{dpm m}^{-2} \text{d}^{-1}$)	at ML depth ($\text{dpm m}^{-2} \text{d}^{-1}$)	Station	Lat	Sampling date	Time elapsed (day)	at 100 m ($\text{dpm m}^{-2} \text{d}^{-1}$)
S1	36.5°S	STZ	21/02/2008	50	926 ± 102	731					
L2	41.2°S	STF	26/02/2008	25	496 ± 57	388					
S2	42.5°S	SAZ	27/02/2008	65	986 ± 87	958	101	42.2°S	13/02/2008	14.9	149 ± 18
L3	44.9°S	SAF	01/03/2008	70	987 ± 86	1118	102	44.4°S	15/02/2008	15.7	530 ± 64
L4	46.0°S	PFZ	03/03/2008	80	871 ± 79	839					
S3	47.5°S	PFZ	05/03/2008	90	1086 ± 104	1086	104	47.4°S	16/02/2008	18.7	447 ± 54
L5	49.0°S	PFZ	07/03/2008	120	1160 ± 102	1521					
L6	50.4°S	PF	09/03/2008	100	1195 ± 120	1195					
S4	51.9°S	SACCF	11/03/2008	120	1073 ± 131	1422	108	51.3°S	19/02/2008	21.1	365 ± 44
L7	55.2°S	AZ	14/03/2008	105	1072 ± 120	1128	118	54.3°S	21/02/2008	22.3	1217 ± 146
S5	57.6°S	WG	16/03/2008	90	800 ± 83	800	125	57.0°S	23.02.2008	22.8	757 ± 91

^aMixed-layer depth determined from the vertical profile of temperature for nearby CTD and taken from Chever et al. (2010).

Title Page

Abstract

Introduction

Conclusions

References

Tables

Figures



Back

Close

Full Screen / Esc

Printer-friendly Version

Interactive Discussion



Late summer
particulate organic
carbon export

F. Planchon et al.

Table 2. Summary of power law fit parameters ($y = aZ^{-b}$; where y represents POC concentrations in $\mu\text{mol L}^{-1}$ and $^{234}\text{Th}_p$ activity in dpm L^{-1} and $Z = \text{depth}$) obtained at five super stations for $>53 \mu\text{m}$ particle during BGH expedition. Fitted values of POC concentration and $^{234}\text{Th}_p$ activity at 100 m and estimated $\text{POC}/^{234}\text{Th}_p$ ratio ($\mu\text{mol dpm}^{-1}$) for $>53 \mu\text{m}$ particles at 100 m.

Station	Zone	depth range (m)	$^{234}\text{Th}_p$			POC			Fitted $^{234}\text{Th}_p$	Fitted POC	POC/ $^{234}\text{Th}_p$
			a	b	r^2	a	b	r^2	(at 100 m)	(at 100 m)	(at 100 m)
S1	STZ	50–2750	0.32	0.66	0.834	1.93	0.88	0.868	0.015	0.034	2.19
S2	SAZ	30–1460	5.23	1.10	0.878	8.03	1.04	0.833	0.033	0.067	2.02
S3	PFZ	20–2040	0.90	0.81	0.869	1.95	0.77	0.835	0.021	0.056	2.62
S4	SACCF	80–2468	2.99	1.08	0.927	28.71	1.19	0.909	0.021	0.120	5.79
S5	WG	50–3894	3.75	1.08	0.775	27.56	1.19	0.824	0.026	0.115	4.43

Title Page

Abstract

Introduction

Conclusions

References

Tables

Figures



Back

Close

Full Screen / Esc

Printer-friendly Version

Interactive Discussion



Table 3. POC export production estimated at 100 m (EP100) in $\text{mmol m}^2 \text{d}^{-1}$ in the SE-Atlantic (BGH section) based on Steady State (SS) and Non Steady-State (NSS) models.

Station	Lat °S	Zone	POC/ ²³⁴ Th ($\mu\text{mol dpm}^{-1}$)		C flux at 100 m ($\text{mmol m}^{-2} \text{d}^{-1}$)			
					SS model		NSS model	
S1	36.5	STZ	1.9	± 0.2	1.8	± 0.3		
L2	41.2	STF	1.8	± 0.3 ^a	0.9	± 0.2		
S2	42.5	SAZ	1.7	± 0.2	1.7	± 0.3	0.3	± 0.0
L3	44.9	SAF	2.4	± 0.7 ^b	2.3	± 0.7	1.3	± 0.4
L4	46.0	PFZ	-	-	2.6	± 0.3 ^e		
S3	47.5	PFZ	3.0	± 0.2	3.3	± 0.4	1.3	± 0.2
L5	49.0	PFZ	-	-	3.5	± 0.4 ^e		
L6	50.4	PF	3.9	± 2.1 ^c	4.7	± 2.6		
S4	51.9	SACCF	4.8	± 1.9	5.1	± 2.1	1.7	± 0.7
L7	55.2	AZ	4.0	± 2.6 ^d	4.3	± 2.8	4.9	± 3.2
S5	57.6	WG	4.1	± 1.7	3.3	± 1.4	3.1	± 1.3

^a mean of STZ (S1) and SAZ (S2) values

^b mean of SAZ (S2) and PFZ (S3) values

^c mean of PFZ (S3) and SACCF (S4) values

^d mean of SACCF (S4) and WG (S5) values

^e calculated using PFZ (S3) POC/Th ratio

Late summer particulate organic carbon export

F. Planchon et al.

Title Page

Abstract

Introduction

Conclusions

References

Tables

Figures

◀

▶

◀

▶

Back

Close

Full Screen / Esc

Printer-friendly Version

Interactive Discussion



Late summer particulate organic carbon export

F. Planchon et al.

Table 4. Details of the Mesopelagic layer thickness; meso-Baxs ($>40\ \mu\text{m}$) in pmol L^{-1} ; O_2 consumption in $\mu\text{mol L}^{-1}\ \text{d}^{-1}$ and mesopelagic respired carbon in $\text{mmol C m}^{-2}\ \text{d}^{-1}$.

Station	Lat	Zone	Cast #	Mesopelagic layer			meso-Baxs ^a pmol L^{-1}	O_2 consumption $\text{J}(\text{O}_2)$ $\mu\text{mol L}^{-1}\ \text{d}^{-1}$	Respired C ^b $\text{mmol C m}^{-2}\ \text{d}^{-1}$
				upper depth m	lower depth m	thickness m			
S1	36.5°S	STZ	23	125	600	475	168	-0.0010	-0.23
S2	42.5°S	SAZ	24	125	600	475	284	0.0040	2.09
L3	44.9°S	SAF	44	123	600	477	497	0.0175	6.39
S3	47.5°S	PFZ	66	124	600	476	305	0.0075	2.50
L5	49.0°S	PFZ	72	125	600	475	388	0.0041	4.16
S4	51.9°S	SACCF	87	120	600	480	235	0.0049	1.11
L7	55.2°S	AZ	99	125	600	475	277	0.0049	1.95
S5	57.6°S	WG	110	123	600	477	271	0.0014	1.83

^a meso-Baxs refers to the depth weighted average of Baxs content integrated over the mesopelagic depth range.

^b Respired C is estimated from the Dehairs et al. (1997) relationship between meso-Baxs and O_2 consumption.

Title Page

Abstract

Introduction

Conclusions

References

Tables

Figures

◀

▶

◀

▶

Back

Close

Full Screen / Esc

Printer-friendly Version

Interactive Discussion



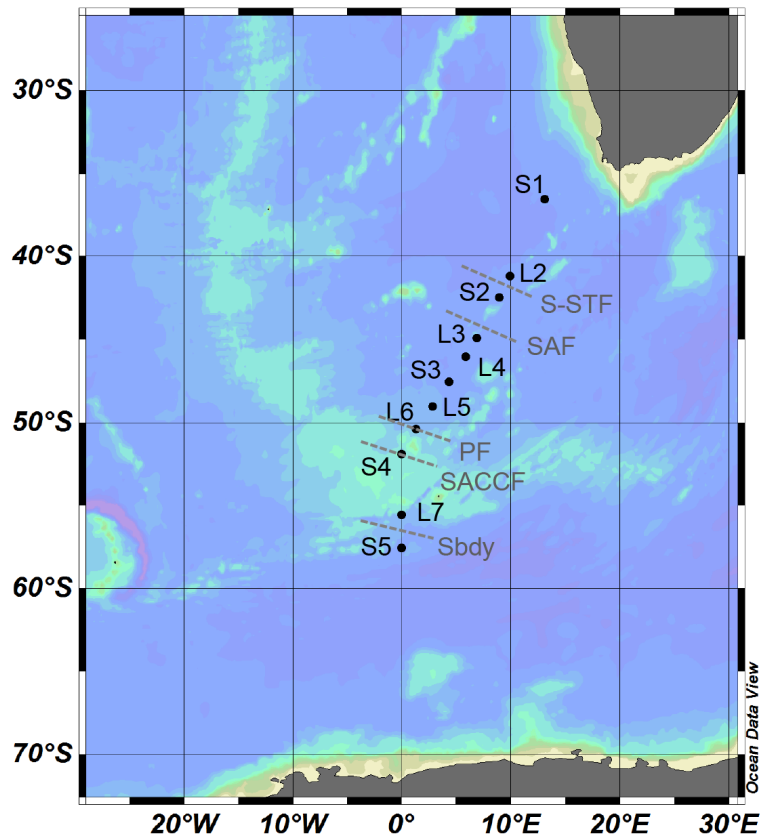


Fig. 1. Cruise track of Bonus-Good-Hope expedition showing position of stations sampled for ^{234}Th as well as frontal zones crossed, including the southern-sub-tropical front (S-STF), the sub-Antarctic front (SAF), the polar front (PF), the southern ACC front (SACCF) and the southern boundary (Sbdy).

**Late summer
particulate organic
carbon export**

F. Planchon et al.

Title Page

Abstract

Introduction

Conclusions

References

Tables

Figures

◀

▶

◀

▶

Back

Close

Full Screen / Esc

Printer-friendly Version

Interactive Discussion



Late summer particulate organic carbon export

F. Planchon et al.

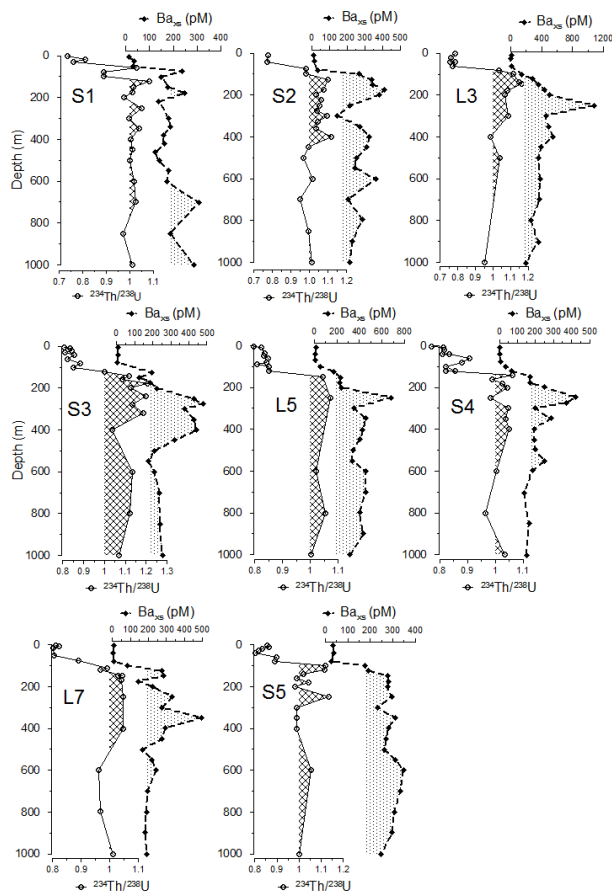


Fig. 2. Vertical distribution of $^{234}\text{Th}/^{238}\text{U}$ ratio and biogenic particulate Ba (Ba_{xs}) in pM along BGH section from the surface to 1000 m depth.

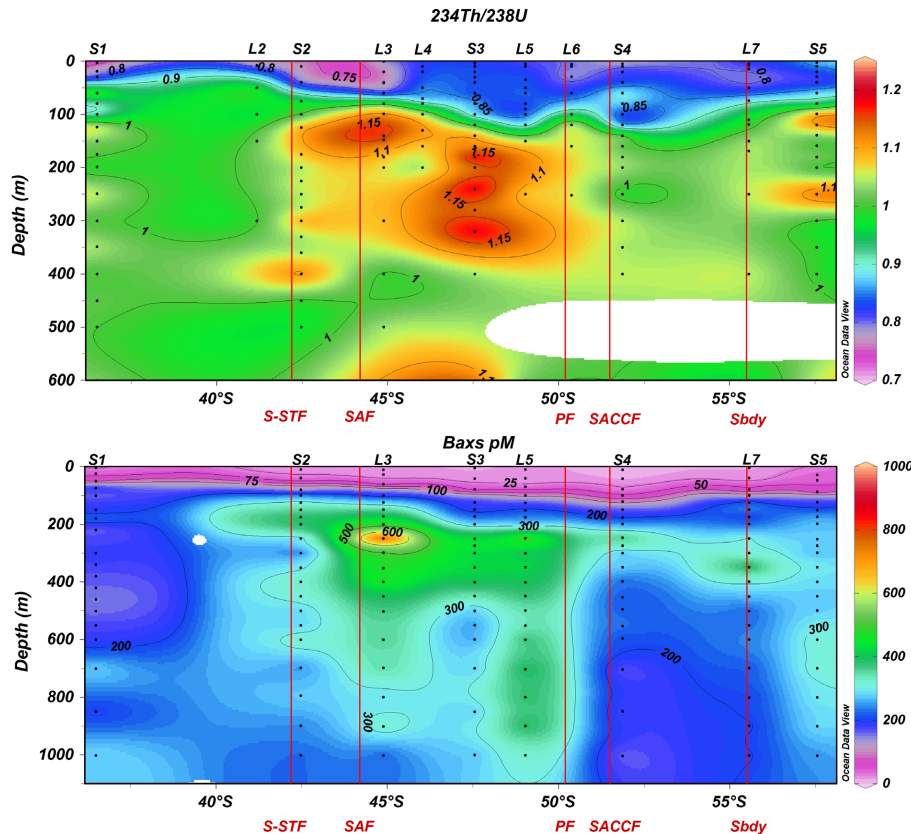


Fig. 3. Latitudinal section of total $^{234}\text{Th}/^{238}\text{U}$ activity ratio in upper 600 m (upper panel) and biogenic particulate Ba in upper 1000 m (Ba_{XS} , lower panel) crossing the subtropical domain, the Antarctic Circumpolar Current (ACC) and the eastern part of the Weddell Sea Gyre.

BGD

9, 3423–3477, 2012

**Late summer
particulate organic
carbon export**

F. Planchon et al.

Title Page

Abstract

Introduction

Conclusions

References

Tables

Figures

◀

▶

◀

▶

Back

Close

Full Screen / Esc

Printer-friendly Version

Interactive Discussion



Late summer particulate organic carbon export

F. Planchon et al.

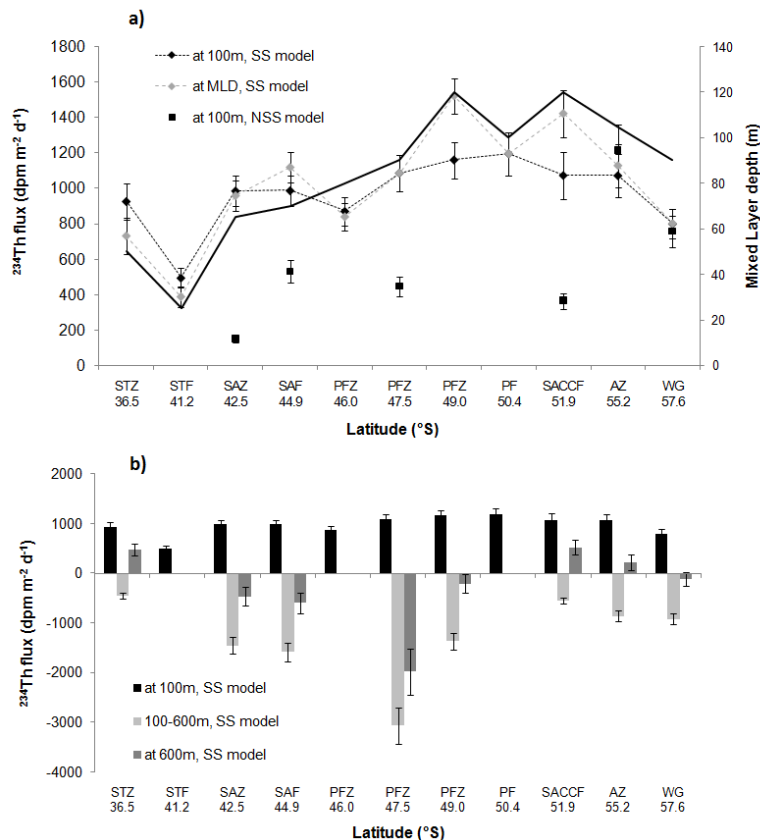


Fig. 4. (a) ^{234}Th export flux ($\text{dpm m}^{-2} \text{d}^{-1}$) at 100 m (black diamonds) and base of the mixed layer (grey diamonds), evaluated using the steady state model, and at 100 m (black squares) using the non steady state model; thick black line = bottom of the mixed layer). (b) ^{234}Th flux ($\text{dpm m}^{-2} \text{d}^{-1}$) at 100 m; between 100 and 600 m and at 600 m calculated using the steady state model.

Late summer particulate organic carbon export

F. Planchon et al.

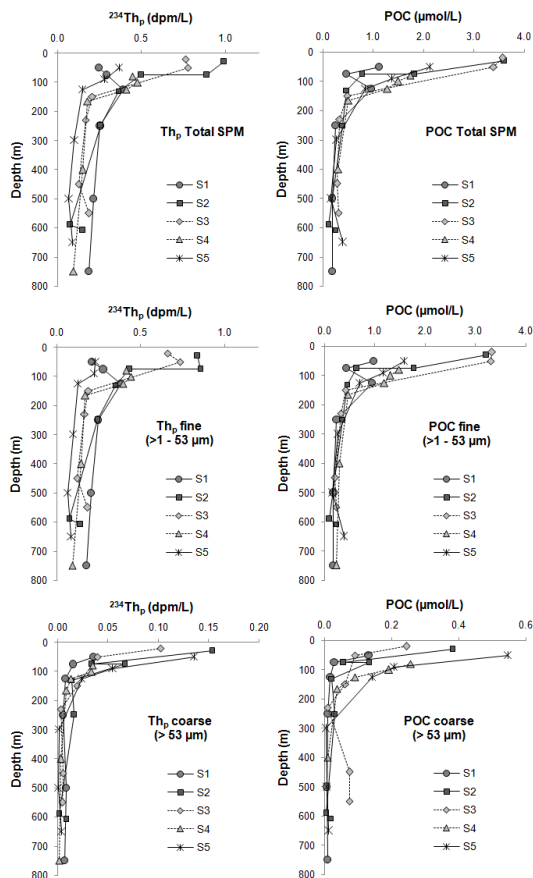


Fig. 5. Depth profiles of particulate ^{234}Th activity (dpm L^{-1}) and POC concentration ($\mu\text{mol L}^{-1}$) for total (>1 μm) suspended material (SPM), and two particle size classes (1 >> 53 μm and >53 μm).

Title Page

Abstract

Introduction

Conclusions

References

Tables

Figures

◀

▶

◀

▶

Back

Close

Full Screen / Esc

Printer-friendly Version

Interactive Discussion



Late summer particulate organic carbon export

F. Planchon et al.

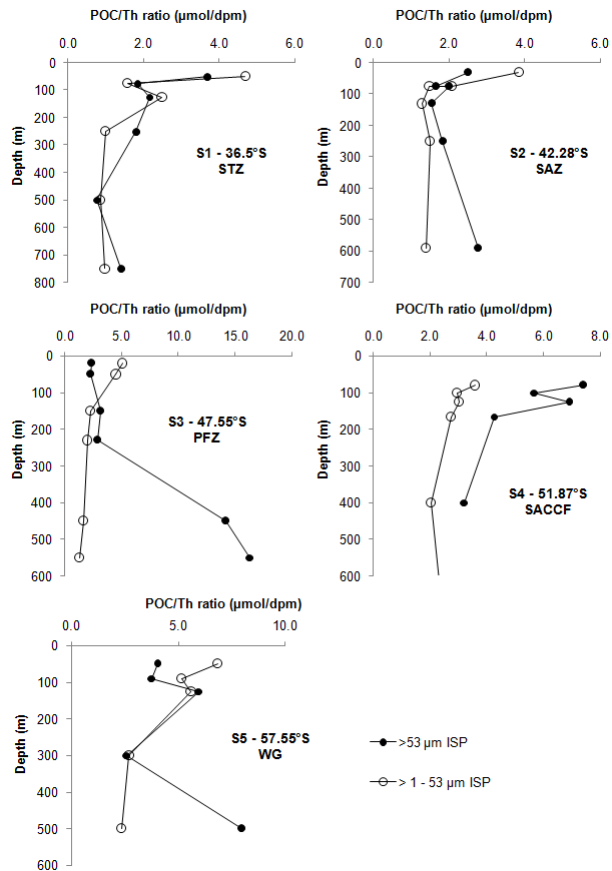


Fig. 6. Vertical profiles of $\text{POC}/^{234}\text{Th}_p$ ratio ($\mu\text{mol dpm}^{-1}$) of $1 \gg 53 \mu\text{m}$ and $>53 \mu\text{m}$ particles for the five super stations (S1 to S5).

Title Page

Abstract

Introduction

Conclusions

References

Tables

Figures

◀

▶

◀

▶

Back

Close

Full Screen / Esc

Printer-friendly Version

Interactive Discussion



Late summer particulate organic carbon export

F. Planchon et al.

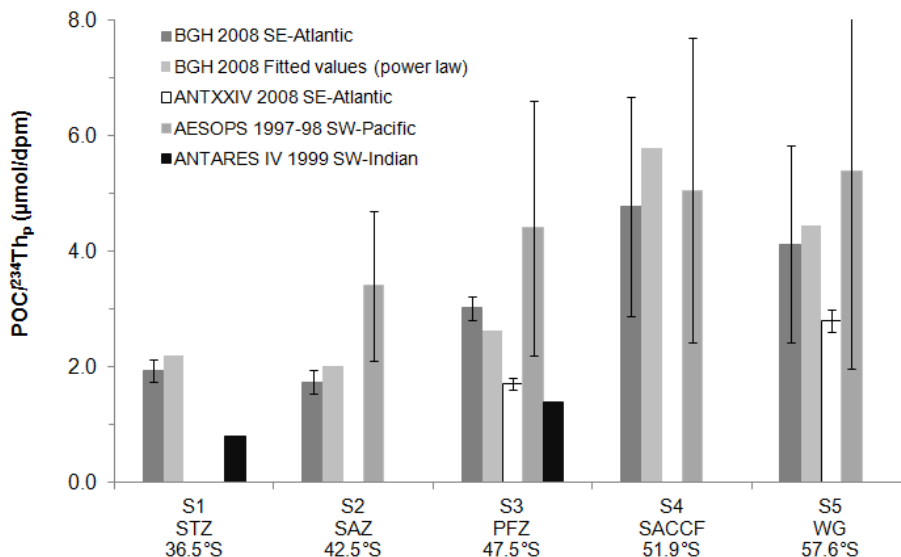


Fig. 7. Comparison of the $\text{POC}/^{234}\text{Th}_p$ ratio ($\mu\text{mol dpm}^{-1}$) of sinking particles ($>53\ \mu\text{m}$) collected at the five super stations (S1 to S5) and calculated from separate power law fits of the POC and $^{234}\text{Th}_p$ profiles (see text for details). Also shown are $\text{POC}/^{234}\text{Th}_p$ ratios ($\mu\text{mol dpm}^{-1}$) reported for the ANTXXIV cruise (Rutgers van der Loeff et al., 2011); the AESOPS cruise in the SW Pacific sector (Buesseler et al., 2001) and the ANTARES IV cruise in the Indian sector (Coppola et al., 2005).

Title Page

Abstract

Introduction

Conclusions

References

Tables

Figures

◀

▶

◀

▶

Back

Close

Full Screen / Esc

Printer-friendly Version

Interactive Discussion



Late summer particulate organic carbon export

F. Planchon et al.

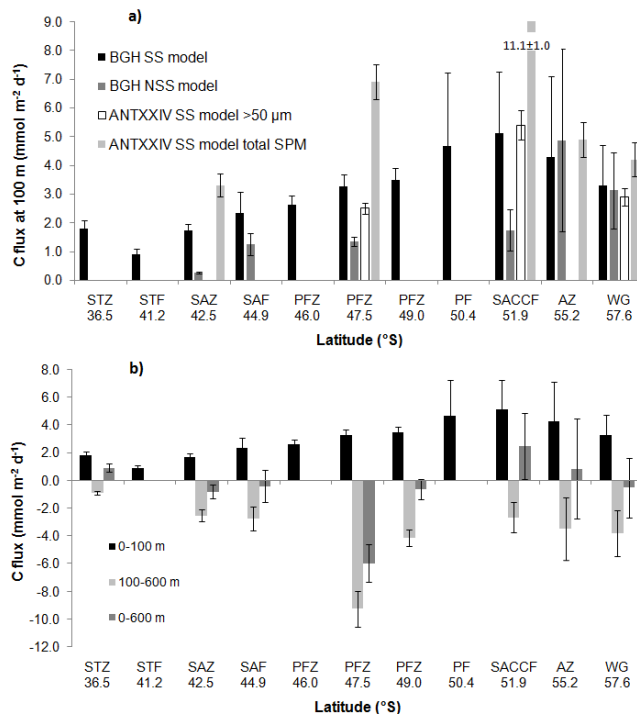


Fig. 8. (a) 100 m-POC export fluxes ($\text{mmol m}^{-2} \text{d}^{-1}$) estimated using SS and NSS models and comparison with POC export ($\text{mmol m}^{-2} \text{d}^{-1}$) from 100 m for $>50 \mu\text{m}$ particles and total suspended material reported for the ANTXXIV cruise (Rutgers van der Loeff et al., 2011). (b) Comparison of the POC export flux from the upper 100 m; the POC flux between 100–600 m (deduced from the ^{234}Th excess activity), and the total integrated POC export from the upper 600 m depth using the SS model.

Late summer
particulate organic
carbon export

F. Planchon et al.

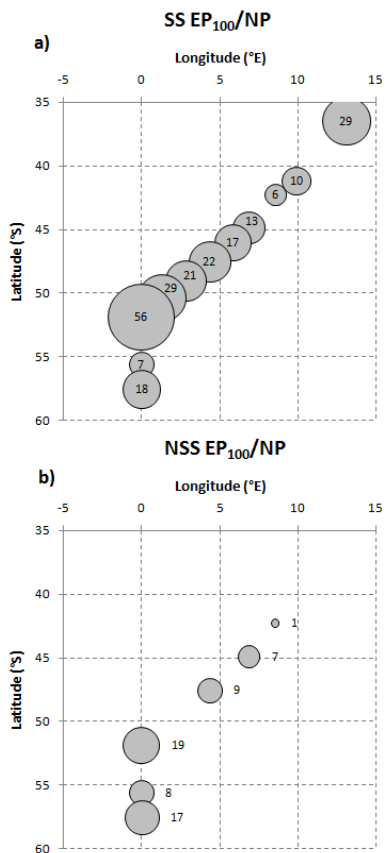


Fig. 9. Bubble plot showing the POC export flux at 100 m based on **(a)** steady state (SS EP100) and **(b)** non steady state models (NSS EP100) as a % of new production (NP) estimated using ^{15}N -labelled nitrate (Joubert et al., 2011). The size of the bubble is proportional to the magnitude of the ratio.

Late summer particulate organic carbon export

F. Planchon et al.

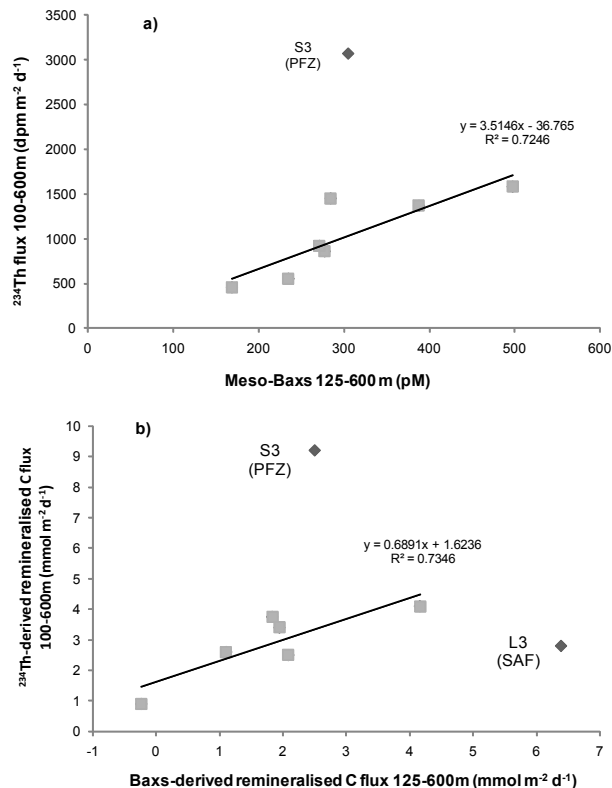


Fig. 10. (a) mesopelagic excess Ba (meso- Ba_{xS} ; μM , 125–600 m) versus mesopelagic ^{234}Th accumulation flux (100–600 m); (b) C remineralisation flux deduced from Ba_{xS} (C_{respired} in $\text{mmol C m}^{-2} \text{d}^{-1}$) plotted versus C remineralisation flux (in $\text{mmol C m}^{-2} \text{d}^{-1}$) deduced from ^{234}Th excess activity in the mesopelagic layer (100–600 m) and the $\text{POC}/^{234}\text{Th}_p$ ratio ($\mu\text{mol dpm}^{-1}$) of $>53 \mu\text{m}$ particles.

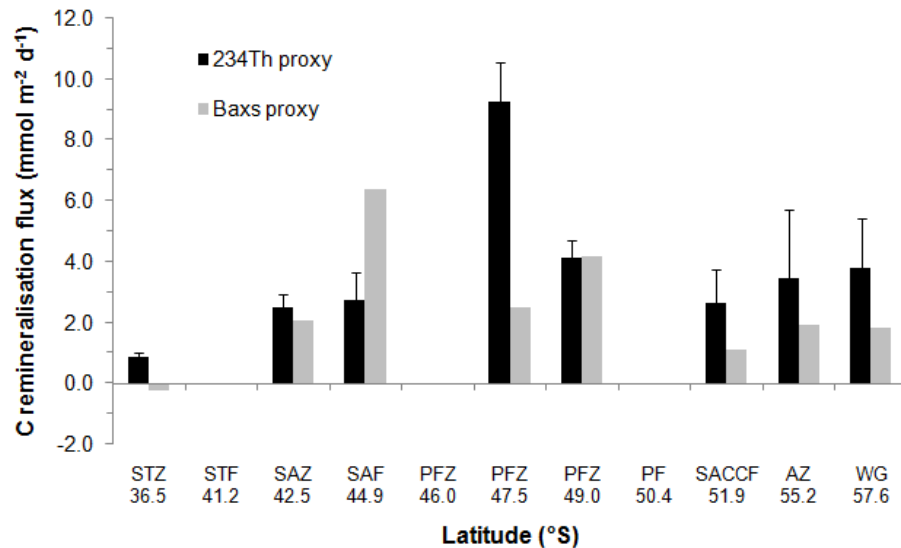


Fig. 11. Remineralisation flux of POC ($\text{mmol m}^{-2} \text{d}^{-1}$) in mesopelagic waters obtained from ^{234}Th and Ba_{xs} approaches.

**Late summer
particulate organic
carbon export**

F. Planchon et al.

Title Page

Abstract

Introduction

Conclusions

References

Tables

Figures

◀

▶

◀

▶

Back

Close

Full Screen / Esc

Printer-friendly Version

Interactive Discussion



Late summer
particulate organic
carbon export

F. Planchon et al.

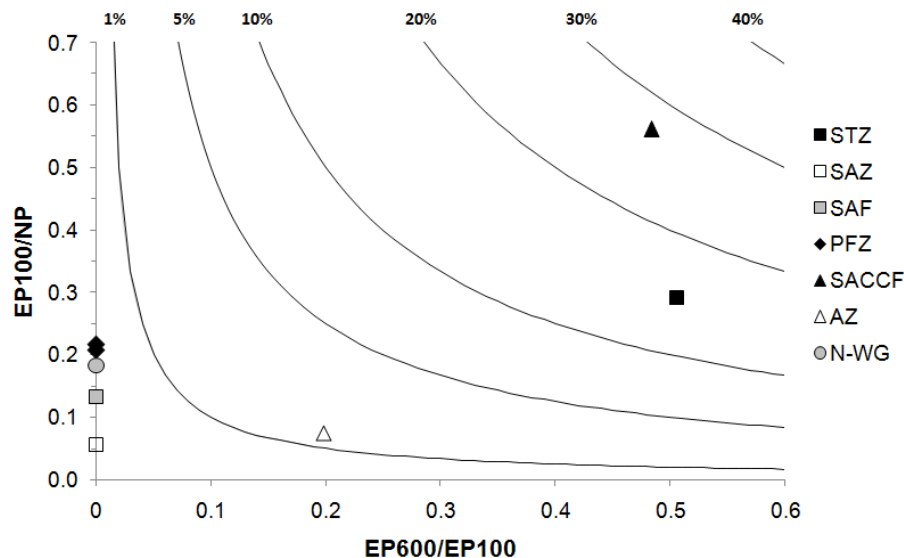


Fig. 12. Ratio of the POC export flux at 600 m over the export flux at 100 m (EP600/EP100) versus the ratio of the export flux at 100 m over New Production (EP100/NP). Isolines represent the modelled 1 %, 5 %, 10 %, 20 %, 30 % and 40 % of NP exported to depths >600 m. Note: EP600 = EP100 – Remineralised C flux; negative EP600 fluxes were set to zero.

Discussion Paper | Discussion Paper | Discussion Paper | Discussion Paper | Discussion Paper

Title Page

Abstract

Introduction

Conclusions

References

Tables

Figures

◀

▶

◀

▶

Back

Close

Full Screen / Esc

Printer-friendly Version

Interactive Discussion

